PAPER

Resolving the controls over the production and emission of ice-nucleating particles in sea spray†

Thomas C. J. Hill, [ID] *[a] Francesca Malfatti, [ID] *[bc] Christina S. McCluskey, [ID] [d] Gregory P. Schill, [ID] [e] Mitchell V. Santander,[f] Kathryn A. Moore, [ID] [a] Anne Marie Rauker,[a] Russell J. Perkins, [ID] [a] Mauro Celussi, [ID] [c] Ezra J. T. Levin,[g] Kaitlyn J. Suski,[h] Gavin C. Cornwell,[i] Christopher Lee, [ID] [j] Paola Del Negro,[c] Sonia M. Kreidenweis, [ID] [a] Kimberly A. Prather [ID] [fj] and Paul J. DeMott [ID] [a]

The role of marine ice-nucleating particles (INPs) in modifying clouds and radiation balance over oceans is uncertain. While recent studies have advanced our understanding of the abundance of marine INPs, characterizing their sources and composition remains a challenge. INP concentrations above oceans are typically low, sometimes extraordinarily so, but there is evidence of elevated levels associated with phytoplankton blooms. Mesocosm experiments have shown that ice-nucleating entities (INEs, which include discrete particles as well as ice-nucleating monolayers) are produced, and INP emissions raised, in the decay phase following bloom collapse. To test if INE production depends upon phytoplankton type, we added dead particulate biomass of a green alga (*Nannochloris atomus*), a diatom (*Skeletonema marinoi*) and a cyanobacterium (*Prochlorococcus marinus*) to a miniature Marine Aerosol Reference Tank filled with seawater. As decomposition progressed, heterotrophic bacteria initially increased and plateaued, then declined, coinciding with an increase in heterotrophic nanoflagellates (HNF) and viruses. Enzyme activities typically increased over several days before plateauing or decreasing, while humic-like substances (HULIS) steadily accumulated. INEs in the seawater peaked 3–5 days after each detritus addition, increasing ~10- to ~20-fold. INE concentration was closely correlated with HNF counts, viruses and the concentration of HULIS, but not with bacteria or enzyme activities. Newly-fabricated INEs were organic, primarily heat stable (95 °C), and varied in size. INP concentrations in sea spray aerosol (SSA) tended to peak shortly before the peak of INEs in the seawater, at 4-, 35- and 15-fold higher than at the start in the *N. atomus*, *S. marinoi*, and *P. marinus* incubations, respectively. Using data from the *P. marinus* incubation, we were able to provide the first estimate of INP enrichment in SSA (over its concentration in the water): it was initially ~200× for the fresh seawater and increased further after the addition of the *P. marinus* inoculum. We also tested if a simple nutrient mix (bovine serum albumin (BSA) and three monosaccharides) could stimulate INP production: INEs in the seawater changed little, but INP emissions fell abruptly immediately upon BSA addition due to it forming a monolayer which displaced the sea surface microlayer (SML). These experiments revealed that INE production in the decay phase of a phytoplankton bloom requires the addition of a natural, complex substrate to initiate a realistic succession of decomposers, and that INP emissions are further controlled by their concentration in the SML and, indirectly, by the impact of SML composition upon jet and film drop production.

[a]*Department of Atmospheric Science, Colorado State University, Fort Collins, CO, USA. E-mail: Thomas.Hill@colostate.edu*

[b]*University of Trieste, Trieste, Italy. E-mail: f.malfatti@gmail.com*

[c]*Istituto Nazionale di Oceanografia e di Geofisica Sperimentale, Trieste, Italy*

[d]*National Center for Atmospheric Research, Boulder, CO, USA*

[e]*Chemical Science Division, Earth System Research Laboratory, National Oceanic and Atmospheric Administration, Boulder, CO, USA*

[f]*Department of Chemistry and Biochemistry, University of California San Diego, La Jolla, CA, USA*

[g]*Handix Scientific, Fort Collins, CO, USA*

[h]*JUUL Labs, San Francisco, USA*

[i]*Pacific Northwest National Laboratory, Richland, WA, USA*

[j]*Scripps Institution of Oceanography, University of California San Diego, La Jolla, CA, USA*

† Electronic supplementary information (ESI) available. See DOI: https://doi.org/10.1039/d2ea00154c

Environmental significance

Oceans emit cloud-active aerosols. One influential class, the ice-nucleating particles (INPs), trigger the freezing of supercooled cloud droplets, reducing cloud reflectivity and longevity whilst facilitating precipitation. Understanding the role of INPs in sea spray aerosols (SSA) is critical for understanding glaciation of marine clouds, especially in remote regions. When phytoplankton blooms collapse, INPs are produced and emitted in the SSA. However, characterizing their sources and dependence upon phytoplankton class remains uncertain. We added dead biomass of three diverse phytoplankton species to seawater in meso-cosms. INP production was stimulated by all species, peaked after 3–5 days, and coincided with increases in nanoflagellates and viruses. Emissions were modified by the sea surface microlayer and its control over jet drop production by bubbles.

1 Introduction

The oceans are a 360 million square kilometre source of cloud-active aerosols. One rare but exceptionally influential class of aerosol is the ice-nucleating particles (INPs). These trigger the freezing of supercooled cloud droplets, which reduces cloud reflectivity and cloud longevity whilst facilitating precipitation. The Southern Ocean (SO) is remote, making long-range transport of INPs from continents of likely minor significance in the marine boundary layer.[1] Consequently, the role of locally-emitted marine INPs is critical for understanding glaciation processes of clouds coupled to the marine boundary layer in such remote regions.

The emissions and impacts of marine INPs are, however, not well understood,[2–4] and discrepancies in simulating mid- and high-latitude southern hemisphere climate[5,6] may be a consequence of this deficiency. Improved knowledge of the energy budget of the SO requires an overall greater understanding of ice formation in SO clouds.[6–10] Earth system models predict "too low cloud optical thickness and/or too low cloud fraction"[5] due in part to them possessing insufficient amounts of supercooled liquid in clouds;[6,9,11] the SO's albedo is particularly sensitive to cloud phase and cover due to the low reflectivity of oceans. The result is a positive bias in modelled absorbed solar radiation at the ocean surface.[5,12] Vergara-Temprado *et al.* (2018)[10] suggest that the cause of the bias is due to modelled SO clouds behaving as if they have higher INP concentrations than actually occur. Indeed, recent measures show that SO cloud tops can be frequently and deeply supercooled,[13] and the boundary layer contain uniquely low INP concentrations[4,14–16] that lie at the low end of the range used for parameterization by Vergara-Temprado *et al.* (2018).[10] While biases in simulated SO short-wave radiative fluxes have improved in recent CMIP6 models,[17] there is a significant diversity in the representation of cloud phase and freezing processes, and their impact on climate.[5–7,9,11,12,18,19] Some studies have demonstrated little influence of ice nucleation on simulated cloud phase and shortwave cloud forcing,[19,20] whereas others have demonstrated a strong relationship between available marine INPs and cloud properties.[21]

Oceans are a generally poor source of INPs. Bulk seawater typically contains $\sim$1–1000 mL^{-1} ice-nucleating entities (INEs include both discrete particles and ice-nucleating monolayers) active at -20 °C,[22–30] a tiny fraction of the number found, for example, in soils (*e.g.*, 10^8 g^{-1} at -20 °C (ref. 31)). Sea spray aerosol (SSA) is also a low efficiency ice nucleator compared with mineral dust.[15,32,34] Accordingly, INP concentrations over oceans are typically two or more orders of magnitude lower than

over land.[3,15,33,34] However, significant and sometimes "phenomenally active"[28] excursions from typical background values in seawater and/or boundary layer air have been recorded, associated with a range of factors, such as higher concentrations of biological material, both dissolved[23,24,30,34,35] and particulate (*e.g.*, gel-like particles),[28,34,35] enhanced productivity in upwelling regions,[36–38] and a reduction in salinity caused by melting sea ice.[23,24] Phytoplankton blooms appear to be large producers of INEs, especially during the microbial succession of bacteria, viruses and protists that ensues when they collapse and their organic matter is re-worked and decomposed.[3,25,29,35,39–41] Emissions of INPs in SSA are also modulated by their enrichment in the sea surface microlayer (SML)[22,24,25,30,42] and by the ratio of jet to film drop production, with the former being a more effective INE ejector.[40,43] Other factors that may enhance INEs in surface waters include deposited dust[35,44] and its stimulation of biological activity *via* iron fertilization.[35]

To further resolve the prerequisites, sources, and controls over emissions of marine INPs, we conducted a series of experiments using a miniature Marine Aerosol Reference Tank (miniMART).[45] We focused on the decaying phase of a phytoplankton bloom, where bacteria colonize and comminute detrital particles produced from freshly-killed phytoplankton. To test if INE production is dependent upon phytoplankton class we added dead biomass of three phytoplankton species, a green alga, a diatom and a cyanobacterium, sequentially to a miniMART, each time filled with fresh seawater containing natural microbial communities. Secondly, to test if INEs can be generated simply by supplying basic nutrients, we added a mix of one protein and three common marine monosaccharides to a miniMART with the same natural communities. Throughout the ensuing decomposer successions, measurements of the bulk water and SSA included: INE/INP concentrations (including after treatments to measure the abundance of organic ice nucleators and of those deactivated by heat); cell counts of bacteria, viruses and grazers; hydrolytic enzyme activities (*e.g.* bacterial degradative activities); 16S rRNA profiling of bacteria; emission-excitation matrices; and aerosol size distributions. Collectively, these experiments revealed the importance of the resource quality of the substrate for INE production, and the composition of the SML and its control over jet drop production, for INP emissions.

2 Materials and methods

We studied the production of ice-nucleating entities (INEs) and its link to the emission of ice-nucleating particles (INPs)

© 2023 The Author(s). Published by the Royal Society of Chemistry

Environ. Sci.: Atmos., 2023, **3**, 970–990 | **971**

induced by the decomposition of organic inputs using the miniature Marine Aerosol Reference Tank (miniMART).[45] The miniMART uses a plunging water jet, which replicates the bubble plumes generated by small waves, and so simulates the meteorological conditions consistent with the occurrence of small whitecaps generated by wind speeds >~3 m s^{-1}. We tested three scenarios: (A) microbial degradation of particulate organic carbon (POC) originating from algal detritus from three species representing major marine algal classes; (B) microbial degradation of dissolved organic carbon (DOC) supplied as a simple protein and monosaccharide nutrient enrichment; (C) Microbial degradation of extant DOC (negative control).

2.1 Experimental design

Seawater was collected at the Ellen Browning Scripps Memorial Pier (La Jolla, CA, 32.86693°N, 117.2573°E) during high tides by filling a 10 L polypropylene cubitainer (Hedwin Division of Zacros America, Inc., pre-cleaned with 1 M HCl and then triple rinsed with deionized water). During filling, water was filtered through a 100 μm Nitex mesh (Sefar). The cubitainer was shipped overnight to Colorado State University (CSU), and the following morning 7.5 L was used to fill the miniMART (total tank volume of 19 L).[45] The fill water was pre-filtered through autoclaved 0.6 μm pore-size polycarbonate filters (Whatman Nuclepore, Cytiva) to remove phytoplankton, that may have produced fresh organic matter *via* photosynthesis, and larger protists (bacterial grazers) and other larger particles present in the seawater.[46] Bacteria, viruses and DOC passed through the filter, as well as some of the small grazers. The miniMART was sealed, the headspace supplied with 6.5 L min^{-1} HEPA-filtered air, and the rotating water wheel started, producing eight 70 mL water jets min^{-1} to generate SSA. The miniMART was kept at room temperature (~23 °C) under low light to prevent growth of any small phytoplankton (*e.g.*, cyanobacteria and picoeukaryotes) that had passed through the 0.6 μm filter. These conditions were maintained continuously for the duration of each experiment.

The tank was left to acclimate for 24 h (designated Day -1), and the following day (Day 0) algal detritus or the nutrient mix was added to simulate either the sudden demise of a phytoplankton bloom or an input of labile organic matter, respectively. Experiments were run for 6–18 days, or once air INP number concentrations peaked. Several measures were taken daily of the tank water and SSA: INE/INP concentrations, bacterial, viral and protist counts, and bacterial degradative activities. Others were taken intermittently at key points: aerosol size distribution, real-time SSA INP concentrations using CSU's Continuous Flow Diffusion Chamber, and water and SSA samples for excitation-emission matrix spectroscopy and DNA extractions.

2.2 Algal detritus preparation and labile organic carbon amendment

Samples of detritus from three species representing diverse groups of marine phytoplankton were prepared for addition to the miniMART (see Table 1). *Nannochloris atomus* (phylum

Table 1 Details of the five miniMART incubation experiments

Amendment	Period	Supplier, strain, medium	Concentration	Notes
Nannochloris atomus detritus	10–16 Feb	Bigelow, CCMP509, f/2 (ref. 54)	14 μg L^{-1} Chl *a* equiv.	Green microalga, phylum Chlorophyta. Has an organic layered cell wall composed of cellulose and other polysaccharides
Skeletonema marinoi detritus	17–26 Feb	OGS, —, f/2 (ref. 54)	2.5 μg L^{-1} Chl *a* equiv.	Diatom, phylum Bacillariophyta. Cells are usually connected in long chains. Cosmopolitan in coastal (not polar) seas, and forms extensive spring blooms. *Skeletonema costatum* was the most abundant phytoplankton species in IMPACTS blooms[39,52]
Prochlorococcus marinus MED4 detritus	30 Aug–9 Sep	Bigelow, CCMP2389, Pro99 (ref. 55)	2.5 μg L^{-1} Chl *a* equiv.	Phylum Cyanobacteria. From eastern Mediterranean. High light adapted. *Prochlorococcus* dominate temperate and tropical oceans
None (control)	23–29 Aug	—	—	Native DOC control
BSA	11–29 Nov	Sigma, A6003	1 mg L^{-1}	Typical DOC in seawater is ~0.5–1.0 mg L^{-1} (ref. 53)
Glucose		Sigma, G7021	0.33 mg L^{-1}	
Galactose		Sigma, G5288	0.33 mg L^{-1}	
Mannose		Sigma, M6020	0.33 mg L^{-1}	

Chlorophyta), *Skeletonema marinoi* (phylum Bacillariophyta) and *Prochlorococcus marinus* MED 04 (phylum Cyanobacteria, *Prochlorococcus marinus* subsp. *Pastoris*, str. CMP1986) cultures were grown under 12/12 h light/dark cycles at 23 °C. Subsequently, the cells were harvested, washed with 0.2 μm-filtered and autoclaved seawater and subjected to seven freeze–thaw cycles[47] to produce algal detritus. The detritus was then washed to remove the dissolved cellular fraction. Prior to harvesting, the chlorophyll *a* (Chl *a*) of each culture was measured[48] to calculate the dose to be added in chlorophyll equivalent units (Table 1). The labile organic carbon amendment was composed of a mixture of one protein (bovine serum albumin, BSA) and three sugars (glucose, galactose and mannose).

INEs were measured in the axenic *N. atomus* and *P. marinus* cultures, but not in the *S. marinoi* detritus, which had been prepared in Italy. After subtraction of INPs in the media, INP concentration was calculated on the basis of chlorophyll equivalent units (Fig. S1†). While *N. atomus* showed very low activity >−24 °C, *P. marinus* appeared to possess some activity extending to around −15 °C. However, since the cultures were not prepared specifically to test for IN activity (*i.e.* after sub-culturing in INE-free media), the apparent activity may have been due to contaminating INEs in the stock inoculum. Ladino *et al.* (2016)[49] tested exudates (exopolymer secretions, but also possibly cellular debris) of *N. atomus* at −40 °C and found they nucleated ice at low RH$_{ice}$ values, but the activated fractions were low. *Skeletonema marinoi* was shown by Alpert *et al.* (2011)[50] to have IN activity at −29 °C, while Ickes *et al.* (2020)[42] measured a T_{50} of ice nucleation in culture samples at approximately −26 to −21 °C; the INEs were also sensitive to a heat treatment. Interestingly, Xi *et al.* (2021)[51] recently measured significant IN activity beginning at ∼−15 °C in a sea ice sample enriched with *Nitzschia stellata*, a diatom from the same class as *S. marinoi*. From its heat sensitivity they suggested the source was a protein-containing colloidal nanogel.

2.3 Bacterial and viral abundance

Seawater was sampled every day and fixed with EM-grade glutaraldehyde at 0.5% final concentration, flash frozen, and stored at −80 °C until flow cytometric analysis was performed (within one month). Heterotrophic bacterial and viral abundances were determined by flow cytometry using a BD FACSCanto™ II (Becton Dickinson). For heterotrophic bacteria and heterotrophic nanoflagellates (HNF), 1 mL of thawed sample was stained with SYBRGreen I at room temperature for 10 min (10^{-4} dilution of the commercial stock) in the dark.[56,57] For viral abundance, 2.5 μL of thawed sample was diluted in freshly prepared 1× TE buffer (pH 8) and stained with SYBR-Green I at 80 °C for 10 min in the dark (5×10^{-5} dilution of the commercial stock).[58] Then, the samples were run at low flow to avoid overlapping events (65 μL for 1 min) through the flow cytometer, and green fluorescence (FL1) and 90° side light scatter (SSC) intensity recorded (the trigger was set on FL1). The samples were weighed before and after the run to measure the analysed volume. Heterotrophic bacteria and viral populations were discriminated based on their signature in the FL1 *vs.* SSC specific cytograms. FL1 threshold was used for bacteria, HNF and viruses.

SSA sampling was done every day by impinging freshly produced SSA into 0.2 μm filtered autoclaved seawater (FASW) at 1 L min^{-1} for 30 min. Five millilitres of the resulting solution were fixed with EM-grade glutaraldehyde at 5% final concentration, flash frozen, and stored at −80 °C until microscopic analysis (within one month). Thawed samples were filtered onto 0.02 μm alumina oxide membranes (Anodisc, GE Healthcare) and stained with SYBRGreen I following the protocol of Noble and Fuhrman (1998)[59] for viral and bacterial estimates. The membranes were then mounted and immediately imaged using an inverted epifluorescence microscope Olympus BX51 with a UPlanFI 100× oil immersion objective equipped with a 490/528 nm excitation/emission filter cube (U-MSWB2). Bacteria and viruses were counted in 20–30 fields.

2.4 Bacterial degradative activities

The bacterial degradative activities of the bulk seawater and SSA samples were measured using fluorogenic substrate analogs at saturating concentrations (20 μM).[60–62] The enzymes alkaline phosphatase (APase, AP), protease (leucine, L), lipase (oleate, O and butyrate, B) and beta-glucosidase (G) were measured with, respectively, substrates 4-methyl-umbelliferyl-phosphate (Sigma, M8883), L-leucine-7-amido-4-methyl-coumarin (Sigma, L2145), 4-methyl-umbelliferyl oleate (Sigma, 75164), 4-methyl-umbelliferyl butyrate (Sigma, 19362) and 4-methylumbelliferyl β-D-glucopyranoside (Sigma, M3633). Fluorescence resulting from enzymatic release of the free fluorophores (4-methyl-umbelliferone (MUF) and 7-amido-4-methylcoumarin (AMC)) was measured by a multimode reader (Synergy™ H1, BioTek) on 96-well microtitre plates incubated in the dark at *in situ* temperature for 1 h. Fluorescence was measured immediately after adding substrates and again at the end of the incubation, at 355 nm excitation and 460 nm emission.

Enzyme activities were expressed as the concentration of substrate hydrolysed per unit time of incubation and normalized by volume of air impinged for SSA samples, or by volume of bulk seawater for water samples. Six replicates for each sample-substrate combination were analysed on the microtitre plate. Standard curves of the free fluorophores AMC and MUF were used to relate fluorescence to free fluorophore concentration. Enzyme activity values for aerosol samples are reported as the difference between the sample and a blank generated by impinging particle-free air in FASW prepared at the beginning of every experiment cycle.

2.5 Measurement of ice-nucleating entities (INEs) and particles (INPs)

2.5.1 Offline measurement using the ice spectrometer. INEs and INPs were measured within a few hours of sampling in water samples and from SSA sampled overnight, respectively. For water samples, ∼10 mL was removed from the miniMART using a sterile disposable pipette and placed in a sterile 50 mL Falcon polypropylene tube (Corning Life Sciences). To sample SSA, two inline filter units (Pall) fitted with 0.05 μm-pore-

© 2023 The Author(s). Published by the Royal Society of Chemistry

Environ. Sci.: Atmos., 2023, **3**, 970–990 | **973**

diameter, 47 mm-diameter Nuclepore track-etched poly-carbonate membranes (Whatman Nuclepore, Cytiva), each overlying a 3 μm-pore-diameter Nuclepore membrane (to provide a clean support), were used. Average flow rate through each filter was 2.75 Lpm, which decreased ~15–30% over the 12–19.5 h periods of sampling. Average volume sampled per filter was 2080 L (1400–2820 L). Details of filter and filter unit cleaning procedures are given in McCluskey *et al.* (2017),[39] except that 0.1 μm-filtered deionized water was used for final rinses. All steps were carried out in a laminar flow cabinet.

To re-suspend collected aerosol, one filter was placed in a 50 mL Falcon tube, 6 mL of 0.1 μm-filtered deionized water added, and the tube tumbled on a Roto-Torque (Cole-Palmer) for 20 min. INEs/INPs were measured in each water sample and aerosol suspension, and in 10- to 20-fold and 225- to 400-fold dilutions of each to estimate concentrations of INEs/INPs active at colder temperatures (to −27 °C). To estimate INPs in each sample and dilution, 32×50 μL aliquots were dispensed into two 96-well PCR trays (Optimum Ultra, Life Science Products) in a laminar flow cabinet, and the trays inserted into blocks of the Colorado State University Ice Spectrometer. Immersion freezing temperature spectra per millilitre of water and per litre of miniMART headspace air were obtained as described in Hiranuma *et al.* (2015),[63] except that the spectrometer headspace was purged with 0.25–1 L min^{-1} of HEPA-filtered and cooled nitrogen, with flow decreasing as temperature was lowered. Ninety-five percent confidence intervals were derived from the frozen fraction of wells at each temperature using formula 2 from Agresti and Coull (1998).[64] For undiluted water samples, freezing temperatures were adjusted by +2 °C to offset freezing point depression caused by salinity. A negative control of 0.1 μm-filtered deionized water was included in each measurement to adjust for INEs in the water used for re-suspensions and dilutions. To account for background INPs on filters, three filter blanks (loaded into inline filter units, which were attached to the miniMART but without flow) were also processed, and a regression derived from the mean INPs per filter at each temperature (background INPs per filter = 5.1 $\times 10^{-6} \times e^{-0.633 \times °C}$, $R^2 = 0.98$). The significance of differences between samples ($p < 0.05$) was assessed using Fisher's Exact Test using counts of wells frozen and unfrozen in each sample to derive exact p values for differences in proportions of wells frozen between samples.

To determine the contribution of heat-labile biological INEs/INPs (*e.g.*, IN proteins), 2 mL aliquots of filter suspensions and water samples were heated to 95 °C for 20 min and then tested in the Ice Spectrometer to estimate the reduction in ice nucleation activity caused by heating. On select water samples, the predominance of organic INEs was assessed by using hydrogen peroxide digestions, followed by analysis in the Ice Spectrometer. Two millilitres of seawater were combined with 1 mL of 30% H_2O_2 (Sigma Aldrich) and the mixture immersed in water heated to 95 °C for 20 min while being illuminated with two, 26 W UVB fluorescent bulbs (Exo Terra) to generate hydroxyl radicals. To remove residual H_2O_2 and prevent otherwise significant freezing point depression, catalase (Cat. No. 100429, MP Biomedicals) was added to the cooled solution until

effervescence completely ceased. Finally, to assess INE size, some samples were filtered with a 0.2 μm syringe filter (DISMIC-13cp, Advantec; pre-rinsed with deionized water and 0.5 mL of sample) and the filtrate used to measure INEs <0.2 μm (*i.e.*, viruses, vesicles and dissolved organic carbon such as cellular debris and cell-free molecules).[65]

2.5.2 Online measurements with the continuous flow diffusion chamber (CFDC). The Colorado State University continuous flow diffusion chamber (CFDC)[66,67] was operated to determine immersion-freezing INP number concentrations in SSA in real-time. The CSU-CFDC is a vertically mounted CFDC with cylindrical walls 1.1 cm apart. The walls are chemically treated to be wettable by water, and each cylindrical column is independently temperature-controlled. To form a thin layer of ice on each wall, the annular gap is flooded with water while each wall is held at approximately −27 °C. After icing, aerosols are introduced into the annular gap *via* a cylindrical knife edge, which is surrounded by a dry, particle-free sheath flow that makes up 85% of the total flow. Both the knife edge and the sheath flow focus the aerosol into a tight lamina, where the temperature and RH can be precisely controlled by adjusting the temperature of each cylindrical column. For operation to target immersion-freezing, the relative humidity with respect to water was set to approximately 105% to ensure that most aerosols activate into droplets. Those droplets that contain INP active at the aerosol lamina temperature or warmer nucleate into ice. The bottom third of the CSU-CFDC consists of a droplet-evaporation section, where the cylindrical walls are held at the same temperature. Here, conditions in the aerosol lamina reduce toward ice saturation, and therefore water subsaturated conditions. Thus, droplets will evaporate in this section while ice crystals will persist. All particles with diameters >500 nm are detected by an OPC at the bottom of the evaporation section, with ice crystals >3.0 μm assumed to be INPs. The CFDC was operated with a 1.5 μm impactor and aerosol diffusion driers in front of the inlet in this study in order to ensure that larger particles were not erroneously counted as INPs.

2.6 Aerosol distribution measurements

Aerosol size distributions were monitored with a scanning mobility particle sizer (SMPS, TSI Model 3080, 0.014 μm < D < 0.75 μm) and an aerodynamic particle sizer (APS, TSI Model 3321, 0.54 μm < D < 20 μm). Aerosol diffusion driers were used to dry aerosol upstream of the SMPS and APS to <20% relative humidity. The SMPS was operated with an aerosol flow rate of 1.0 Lpm and sheath flow rate of 3 Lpm. The APS inlet has a total flow rate of 5 Lpm, consisting of a 1 Lpm aerosol flow pulled through an inner nozzle surrounded by sheath flow (4 Lpm). Due to flow restrictions of the miniMART system, the APS configuration used a sampling inlet that pulled 1 Lpm from the miniMART and 4 Lpm filtered sheath flow from the room. Several corrections were applied to the APS data: a size calibration using polystyrene latex spheres of known sizes was applied, the first three size bins of the APS were removed due to poor counting statistics, and the particle density of SSA was

974 | *Environ. Sci.: Atmos.*, 2023, **3**, 970–990

© 2023 The Author(s). Published by the Royal Society of Chemistry

assumed to be 1.8 g cm^{-3} (ref. 68) to convert aerodynamic diameter to physical SSA diameter (shape factor assumed to be 1). The last 11 size bins were removed from the SMPS distributions due to poor counting statistics and the impactor 50% cut-off ($D_{50} = 700$ nm). These corrected SMPS and APS data were then merged to form the aerosol size distribution. Aerosol surface area was calculated assuming a spherical shape for all particles.

2.7 Fluorescence excitation-emission matrix (EEM) spectroscopy

EEM spectroscopy was used to characterize and obtain relative concentrations of fluorescent organic compounds in tank water and SSA on key days in each succession. EEMs were obtained for all samples using a spectrofluorometer (Horiba Scientific, Aqualog). Excitation wavelengths ranged from 235–450 nm, and emission from 250–800 nm. A background spectrum acquired with ultrapure water was subtracted from all EEMs. EEMs were corrected for inner-filter effects, and Rayleigh scatter (1st and 2nd order) was removed. EEMs were also normalized to the area of the Raman Scattering peak of water at 350 nm excitation to convert fluorescence intensities to Raman Units (R.U.). For aerosol samples, Raman Units were adjusted to a constant volume of filtered air (1 m^3). Fluorescent regions included those indicative of humic-like substances (excitation/emission ranges: 360/445–460 nm, 260/425–475 nm, and 320/400–420 nm), tryptophan-like (excitation/emission: 235/329 nm), tyrosine-like (excitation/emission: 235/302 nm) and an unusual protein-like peak with an excitation peak at 240 nm and an emission range of 300–350 nm.

2.8 DNA sequencing and diversity analyses

Next-generation sequencing of the bacterial 16S rRNA gene was performed on DNA extracted from tank water and SSA in the *N. atomus* detritus addition experiment. DNA was extracted from frozen tank water from days 2 and 3, and from SSA filtered overnight on days 1 → 2 and 2 → 3, corresponding to one day prior to and the date of peak INP concentrations. For water samples, 6 mL was centrifuged at 20 000×g for 5 min, the supernatant removed, and the remaining 50 μL used for DNA extraction. For SSA, half a filter was cut into strips and these were added directly to the bead beating tube. DNA extraction was performed using the DNeasy PowerLyzer Microbial Kit (QIAGEN), with homogenization by bead beating using a Fast-Prep-24 instrument (MP Biomedicals). DNA was extracted using the high recovery modification of the standard method as detailed in Hill *et al.* (2014).[69] All procedures were carried out using sterile utensils in a laminar flow cabinet. The centrifuge, bead beater and pipets were cleaned with DNA AWAY (MBP).

Sequencing was performed by the Joint Genome Institute using Illumina MiSeq paired-end sequencing of the V4–V5 region of the 16S rRNA gene using primers 515F-y and 926R (Parada *et al.* 2016).[70] Sequencing generated 1.2–1.5 million reads per sample. Percent of reads with an average base calling Phred quality Q score >30 was >80%. iTagger v2.1, which uses Usearch and Qiime to analyse amplicon libraries, was used for processing. Contaminants were essentially all chloroplast or mitochondrial rRNA. Operational taxonomic units (OTUs) were clustered using a 97% identity threshold. Classification primarily used the taxonomy report integrated within the National Center for Biotechnology Information's Basic Local Alignment Search Tool (BLAST), and the Seqmatch tool of the Ribosomal Database Project, Release 11.[71]

Basic diversity analyses were performed on each dataset. To estimate total OTUs we used Chao 1, a non-parametric estimator that uses the number of singletons and doubletons to predict total OTU abundance. In practice it provides a lower limit of total diversity. Two general measures of diversity were chosen:[72] the Shannon index (H'), a measure of the difficulty in predicting the identity of the next individual sampled, which is positively correlated with both species richness and evenness, giving more weight to rare than common species; and the log series index (α), which requires only total number of species/OTUs (S) and total counts (N) to calculate and is a fitted constant in the equation describing the log series model of species abundance. α responds approximately exponentially to changes in S/N ratio and was recommended by Magurran (1988)[73] as a possible universal diversity statistic. We also calculated Simpson's index (D), which gives the probability that two sequences chosen at random will be from the same OTU. It gives a strong weighting to the dominants, with a higher value indicating lower diversity. Principal components analysis was performed using a correlation matrix of standardized scores with missing values excluded pairwise.

3 Results and discussion

Each experiment was initiated with seawater that had been 0.6 μm-filtered to remove particulate organic carbon (POC).[74,75] Ammerman *et al.* (1984)[46] reported that about 70% of bacteria in Scripps Pier seawater were ≤0.6 μm in diameter, and all passed through a 1 μm filter (*i.e.*, would pass through the not uncommon coincident multiple holes in the 0.6 μm membranes). Hence, filtering will have left the standing bacterial community largely intact. The starter filtrate thus contained bacteria, viruses, vesicles[76] and "a broad, polydisperse mix of biopolymers, including polysaccharides, proteins, nucleic acids, and lipids".[75] Dead algal biomass, or a simple nutrient mix comprising one protein and three monosaccharides, was then added to simulate the pulse of decomposable organic matter that follows the collapse of a phytoplankton bloom, initiating a microbial succession. We present the results in decreasing POC → DOC ratio. That is, three experiments involving the addition of algal POC followed by one experiment in which a protein + monosaccharide DOC nutrient mix was added.

3.1 Changes in the seawater during incubations

3.1.1 Microbial dynamics and INP production in seawater. In the three experiments in which algal detritus was added, we observed similar changes in general microbial composition (Fig. 1). As decomposition progressed, heterotrophic bacteria

© 2023 The Author(s). Published by the Royal Society of Chemistry

Environ. Sci.: Atmos., 2023, **3**, 970–990 | **975**
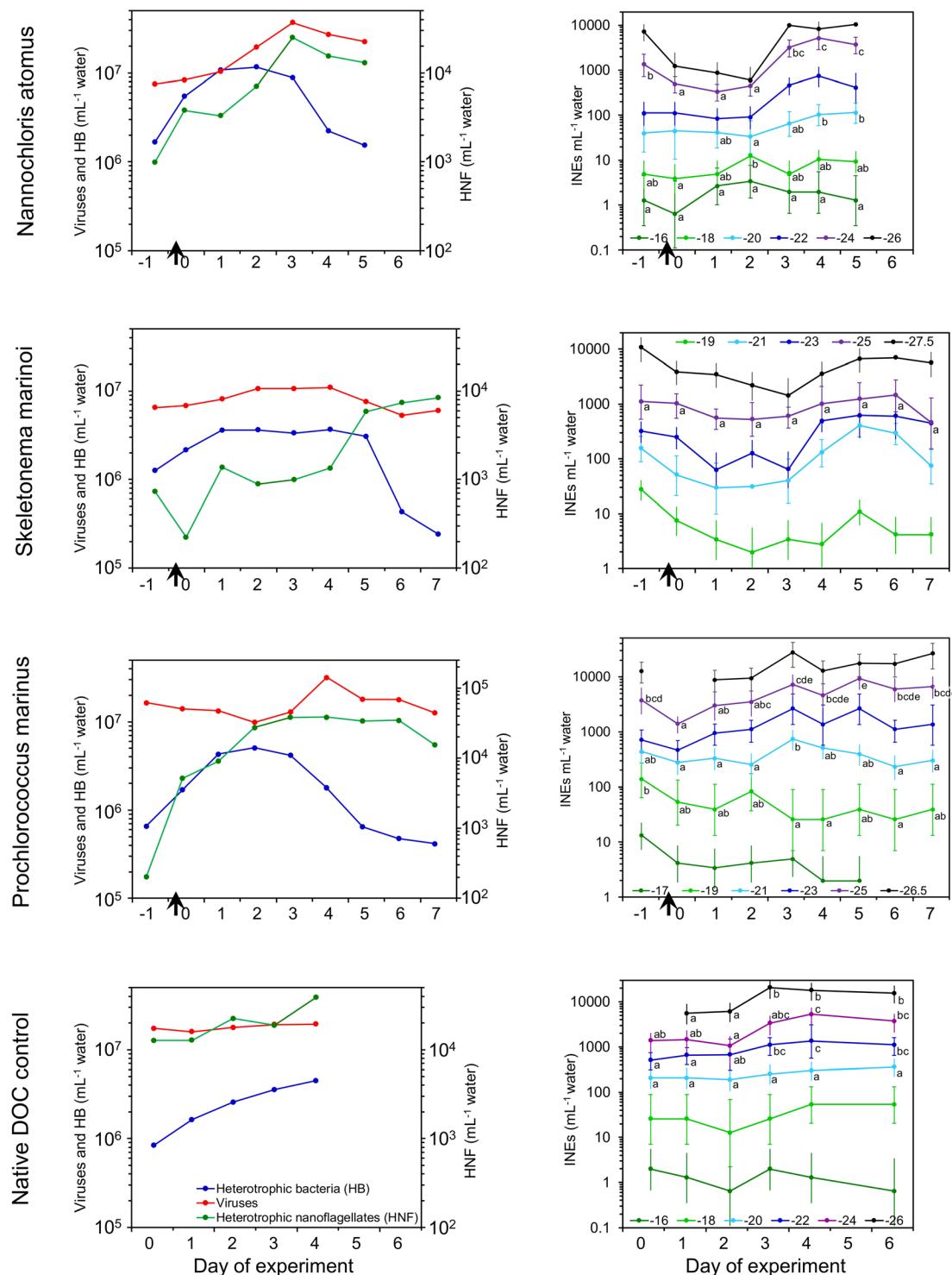
Fig. 1 Changes in microbial abundances and INEs in seawater to which algal detritus had been added (at arrow), and in a no-addition control. For INE spectra, bars show 95% confidence intervals. For selected INE spectra, pairwise Fisher's exact tests were used to assess the significance of changes (points sharing the same letter are not significantly different; $p = 0.05$).

bloomed over two days before plateauing. After several more days, bacterial populations decreased rapidly, which coincided with an increase in heterotrophic nanoflagellates (HNF, a seed population of which had also passed through the coincident multiple holes) and, in two cases, viruses. Enzyme activities

typically increased over the first 1–3 days before plateauing or decreasing (Fig. S2†), which suggested an intense re-working of all the component fractions of the algal-derived POC (e.g., lipids, carbohydrates, proteins). Humic-like substances (HULIS), being harder to degrade,[77] steadily accumulated

(Fig. S2†), as also observed by Lee *et al.* (2015).[78] In the negative control incubation, comprising solely filtered seawater, the change principally comprised the re-growth of bacteria (Fig. 1) on the existing DOC.

INEs in the water initially decreased or remained level (Fig. 1). Note that the added detritus itself contained few INEs (Fig. S1†). After 1–4 days, INE concentrations rebounded, increasing by up to 18-, 14- and 7-fold in the *N. atomus*, *S. marinoi*, and *P. marinus* incubations, respectively. Increases tended to be confined to INEs active below −20 °C. Interestingly, there was also a 5-fold increase in INEs active below −22 °C in the control incubation, driven by the native DOC in the seawater.

3.1.2 Size, heat stability and organic INE abundance. INEs in the fresh seawater at Day 0 were predominantly organic, as shown by their removal after H_2O_2 digests (Fig. S3†). Later, at their peak day, the relative decreases following H_2O_2 digestions were greater, confirming that the newly-formed INEs fabricated by the microbiota were also organic.

Heating the seawater to 95 °C to denature biological INEs produced small changes (Fig. S3†). In fresh, 0.6 μm filtered seawater, INEs active above ∼−22 °C were heat sensitive in two of the incubations, as also found in McCluskey *et al.* (2018),[25] but at peak days the populations were generally unaffected by it, indicating new INEs weren't proteins.

Testing of filtrates after 0.2 μm filtration produced varied effects (Fig. S3†). At Day 0, three of the incubations (*S. marinoi*, *P. marinus* and the control experiment) had significantly lower INE concentrations in the filtrate, indicating most were >0.2 μm and therefore potentially bacteria, grazers or INEs within microgels. At peak INE days different patterns had emerged: the *S. marinoi* INE population was uniformly <0.2 μm (*i.e.*, viruses, vesicles, cellular debris and/or cell-free molecules), the *P. marinus* and control experiments had INEs both smaller and larger than 0.2 μm, with cross-overs occurring at ∼−22 °C, while the *N. atomus* INEs were all >0.2 μm. This variation suggests that different INE sources developed in different incubations. McCluskey *et al.* (2018)[25] found most INEs were >0.2 μm in a waveflume bloom, persisting throughout that entire 5 weeks experiment.

3.1.3 General correlations. To assess general correlations across all experiments, including the control, Principal Components Analysis was performed (Fig. 2a). The INE concentration at −23 °C was used since it was mid-range and responsive in all experiments. The first two components accounted for 72% of the variance, and the INE eigenvector was most closely correlated with HNF counts, but also to viruses and the concentration of HULIS. Notably, no overall correlation existed between INEs and bacterial concentrations. To further explore the relationship between INEs and grazers, their relative changes during each succession are shown in Fig. 2b. Over time, both populations increased in a roughly 1 : 1 ratio, which was also evident in the control experiment since, as mentioned, the filtered water contained enough DOC to initiate a modest succession.

Heterotrophic nanoflagellates are protist grazers, 2–20 μm in diameter and possessing flagella. They are the main predators of bacteria, which they consume *via* a process called phagocytosis. If the HNFs are the primary source of the INEs then this could arise directly from IN-active molecules associated with HNFs, or indirectly *via* their production of IN-active bacterial decomposition products or the fragmentation of pre-existing INEs in the consumed bacteria. If viruses drive INE production it could occur, similarly, *via* growth of an IN phage population or *via* bacterial lysis and disintegration producing an apparent multiplication of INEs. The proliferating HNFs and viruses produce new organic matter pools, with one fraction being ready utilizable[79,80] and the other more recalcitrant, possibly funnelling into the HULIS pool. Fragmentation and dispersal of INE-containing entities was suggested as the principal mechanism of apparent proliferation by Wilbourn *et al.* (2020).[81] Indeed, during the *P. marinus* incubation the
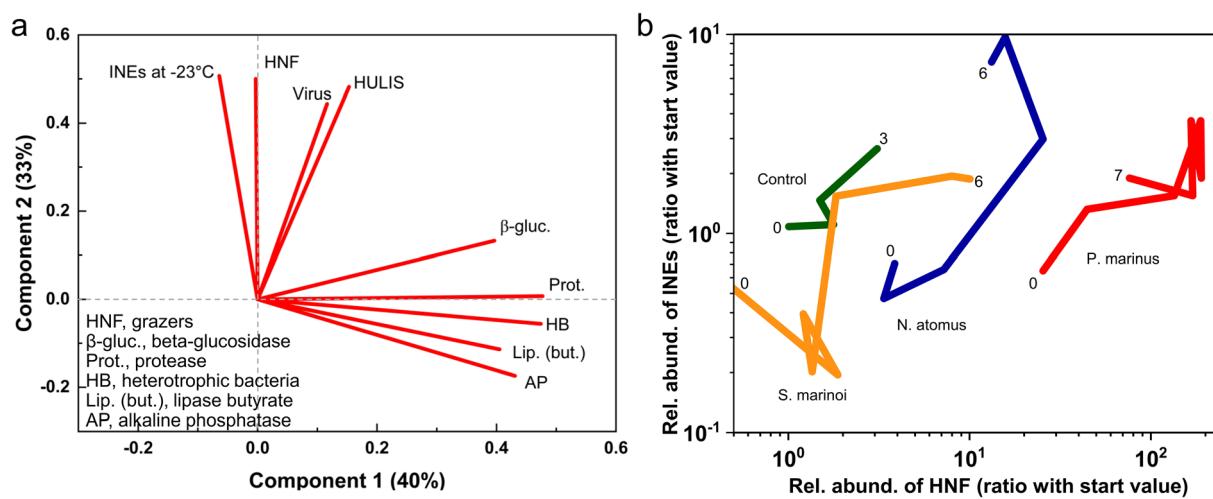
Fig. 2 a) Principal Components Analysis of generalized relationships across all experiments. (b) Relationship between HNF grazers and INEs (active at −23 °C) in seawater during the miniMART experiments. Relative abundances are standardized using the ratio of the value at Day "*x*" and the value at the start of each experiment (Day -1, before the addition of detritus). Numbers indicate day of incubation.

© 2023 The Author(s). Published by the Royal Society of Chemistry

Environ. Sci.: Atmos., 2023, **3**, 970–990 | **977**
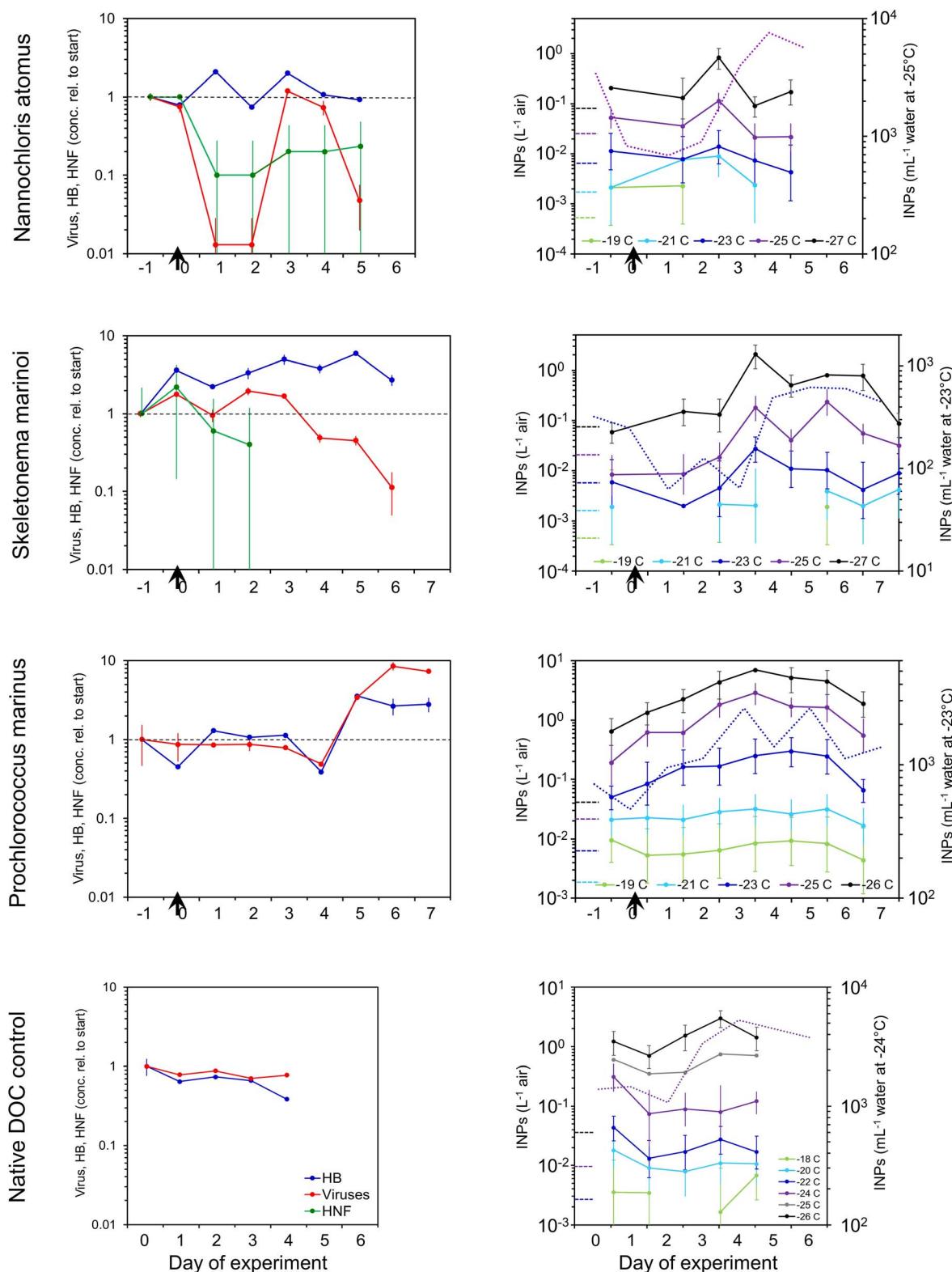
Fig. 3 Changes in microbial populations and INPs in SSA during incubations of seawater to which algal detritus had been added (at arrow), and in a no-addition control. Microbial numbers are shown relative to their concentrations in the headspace of the miniMART at the start of each incubation. For INP spectra, solid lines are concentrations in the SSA while the dashed line shows INE concentrations in the water at the temperature at which INE response was greatest. Error bars that exceed the borders of the graphs extend to zero.

978 | Environ. Sci.: Atmos., 2023, 3, 970–990

© 2023 The Author(s). Published by the Royal Society of Chemistry

disappearance of remnant intact (countable) *P. marinus* cells coincided with INEs increasing in the water.

3.2 Changes in SSA emissions during incubations

3.2.1 INPs and microbes in SSA. Bacterial emissions tended to be stable (Fig. 3), apart from increasing in the latter half of the *P. marinus* experiment, and were broadly paralleled by viral counts, apart from in the *N. atomus* incubation. Enzymes were detected in the SSA (Fig. S4†), typically intermittently, with lipase butyrate possessing the highest activity.

Changes in concentrations of INPs in the SSA generally paralleled those in the water (Fig. 3). INP concentrations in the SSA peaked three to four days after the addition of detritus, being 4-, 35- and 15-fold higher than emissions at the start in the *N. atomus*, *S. marinoi*, and *P. marinus* incubations, respectively. These increases were seen in INPs active below around −24 °C. Paralleling the INPs, HULIS and protein-like substances peaked in the middle of the *N. atomus* and *S. marinoi* incubations, before declining (Fig. S4†).

In previous waveflume and mesocosm studies, INP emissions in SSA were seen to increase, similarly, by 13- and 30-fold three to four days after the collapse of a phytoplankton bloom with the resulting injection of decomposable biomass.[39]

There were differences in INE and INP dynamics in the SSA and water : SSA INP emissions tended to peak a day or so earlier than in the water and, in at least two cases, decline faster. These differences could be caused by several mechanisms, all mediated by the interaction between the INEs and the SML. Firstly, the characteristics (*e.g.*, hydrophobicity) of the INEs may have changed over time, with the initial INE population being more enriched in the SML, and hence emitted, than those predominating later. Secondly, enmeshment of INEs within aggregating gels may have curtailed INP emissions after a couple of days due to the increasing size of the gels reducing their likelihood of being ejected. Enmeshment of INEs within growing gels would manifest itself as an apparent increase in INE size and, therefore, a reduction in INEs passing through a 0.2 μm filter. This was evident in the *N. atomus* incubation (Fig. S3†), but not in the *S. marinoi* incubation. However, both showed peak SSA INP emissions a day earlier than in the water. Thirdly, changes in SML composition and thickness may have altered INE emissions. The effect of this may have been directly linked to increased INE enrichment within the SML, and/or indirect and caused by changed bubble longevity affecting the time for enrichment of INEs in films or a shift in bubble size altering the relative abundances of film *vs.* jet drops.

Heat tests (95 °C) on aerosol INP samples produced minimal changes (Fig. S5†), similar to the results in the water (a lack of available suspension precluded other tests). The only consistent impact occurred in the control experiment where, just as in the water, a modest reduction was apparent at Day 2–3, suggesting the INPs were predominantly biological. By contrast, previous waveflume SSA emissions showed a more general INP heat sensitivity, especially for those active above −20 °C.[25]

3.2.2 Heterotrophic bacterial composition and emissions during the *N. atomus* addition experiment. We profiled the bacteria in the water and SSA during the *N. atomus* addition experiment to assess indicative changes in community composition and OTU emission efficiencies during the period of peak INP emissions. Profiling OTU emissions was also intended to detect known IN-active bacteria in the SSA. Both aspects may affect INP concentrations, the former *via* changes in relative abundances of OTUs in the SSA and water indicating changes in SML composition that impacted emission efficiencies, and the latter from the direct contributions from IN bacteria. Sequencing was performed over the peak period of INP emissions, on days 2 and 3 in the water, and in overnight SSA filter collections on days 1 → 2 and 2 → 3, which corresponded to one-day-prior-to and peak INP emission periods, respectively.

Among all samples, a total of 317 OTUs were detected. The Chao I estimator, which provides a lower limit of total diversity,[82] predicted ∼210–230 OTUs in each of the four samples (Table S1†). The somewhat greater diversity detected in the SSA samples was reflected in their higher log series (α) and Shannon index (H') values; H' is positively correlated with both species richness and evenness. The presence of some very dominant OTUs in all samples generated relatively high Simpson's dominance index (D) values.

The identities and relative abundances of the more common OTUs (average relative abundances >0.1%, or >0.2% in a single sample) in the water and SSA are given in Fig. 4 and Table S2.† Three phylogenetic groups, which accounted for 51/54 of the most abundant OTUs in the water (Fig. 4), are found to consistently dominate bloom-associated bacterial communities.[83–87] They are the Rhodobacteraceae within the Alphaproteobacteria, the Gammaproteobacteria, such as members of the Alteromonadaceae, and the Flavobacteriia class within the Bacteroidetes. Several of the most abundant genera (*e.g.*, *Pseudofulvibacter*, *Methylophaga*, *Vibrio*, *Glaciecola*) have also been recorded as predominating in natural successions in hydrocarbon/biomass-enriched or bloom-associated environments[88] and mesocosm experiments.[52,85,89,90]

Several OTUs were particularly notable. A *Marinobacterium* sp. (OTU 0) was very abundant in the water, while OTU 2, a *Methylophaga* sp., increased greatly in relative abundance in the water between days 2 and 3 while maintaining a relatively low emission efficiency (Fig. 4). In contrast to the *Marinobacterium* and *Methylophaga* spp., a species of *Pseudofulvibacter* (OTU 1) was extraordinarily enriched in the aerosol while comprising only 0.01% of seawater sequences (Fig. 4). Explanations for the dominance of these species and why the Flavobacteriia predominated among OTUs enriched in the SSA (Fig. 4) are given with Table S2.†

Several OTUs increased greatly in their relative abundances in both the water and SSA over the 24 h period (Fig. 4). Most marked were the *Methylophaga* sp. (OTU 2), two *Piscirickettsiaceae* spp. (OTUs 16 and 34), an *Alphaproteobacteria* sp. (OTU 46) and a *Cryomorphaceae* sp. (OTU 20). In general, however, the ratios of the relative abundances in the SSA and in the water remained fairly constant.

None of the genera or families that showed marked increases have been associated with ice nucleation in previous studies. Of the known ice nucleation active bacteria (the genera

© 2023 The Author(s). Published by the Royal Society of Chemistry

Environ. Sci.: Atmos., 2023, **3**, 970–990 | **979**
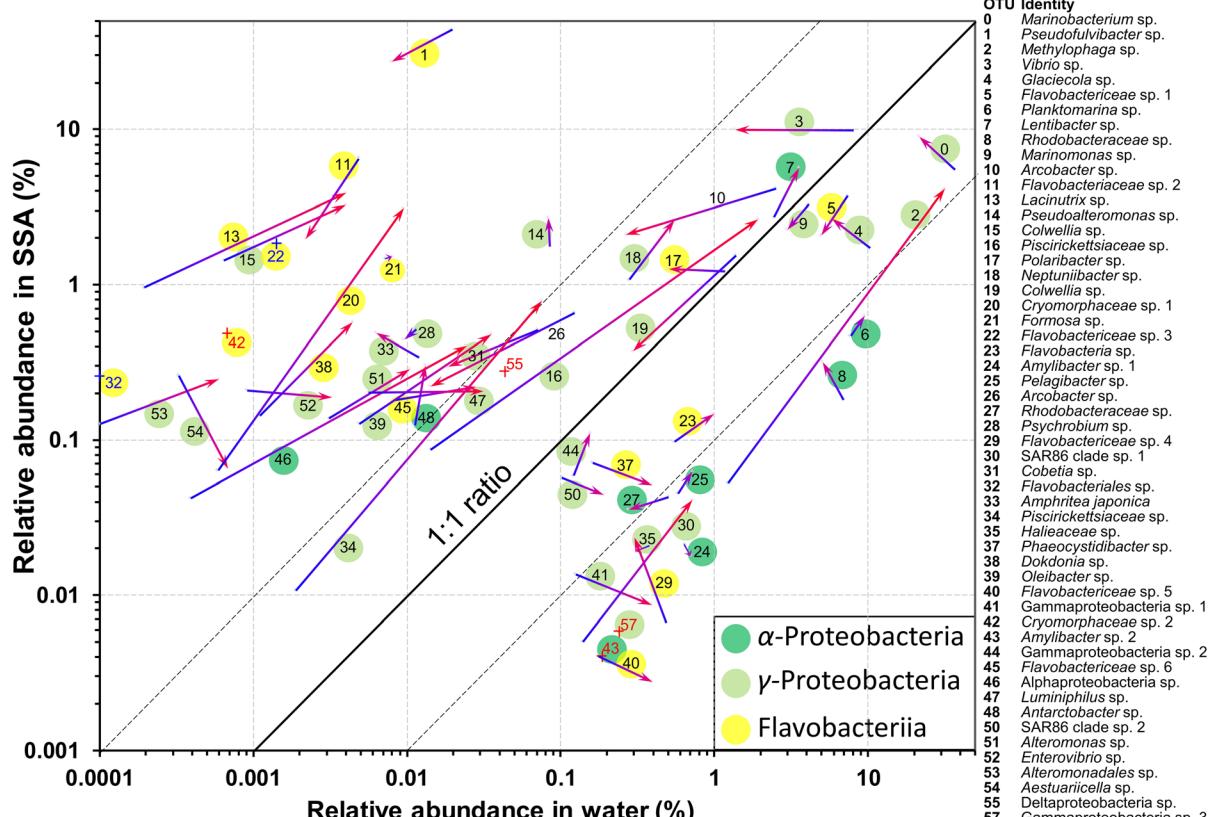
Fig. 4 Relative abundances of the most abundant OTUs in seawater and SSA over the peak period of INP emissions during the *N. atomus* addition experiment. Arrows show changes in relative abundances of OTUs over the 24 h. OTU labels are beside arrows. Red numbers indicate OTUs for which one of the abundance measures was outside of the ranges shown. The three bacterial classes that dominated the community are indicated by coloured circles around the label.

Pseudomonas, *Xanthomonas*, *Pantoea* and *Lysinibacillus*) only one potential species, a Pseudomonad (OTU 88), was recorded. However, it was barely detectable, with only 3 reads among a total of >2.5 million in the two water samples.

3.3 Pure nutrient addition experiment

We also tested whether adding a simple DOC mix could initiate the production of INPs, mimicking the surge of DOC expected during the death phase of a phytoplankton bloom. This experiment is treated separately from the other incubations because it used an unrealistically simple and easily metabolized cocktail and higher DOC concentration ($\sim 2\times$ than is typical in seawater), and so will have stimulated the growth of an atypical and opportunistic subset of heterotrophic bacteria. The labile DOC amendment was composed of one protein, bovine serum albumin (BSA, 1 mg L^{-1}), plus three sugars (glucose, galactose and mannose each at 0.33 mg L^{-1}) that are common in both marine colloids and bulk seawater.[75] The response of the decomposer community was similar to the previous incubations (Fig. S6†) except that a collapse in heterotrophic bacteria, typically coincident with a surge in nanoflagellates, was not seen. INE numbers remained unchanged apart from a modest increase at lower temperatures. The INEs were predominantly organic, heat resistant and <0.2 μm.

In contrast to their stability in the water, INP emissions in the SSA decreased dramatically immediately upon nutrient addition (Fig. 5). The suppression was caused by the formation of a monolayer, ~ 4 nm deep, of protein adsorbed at the air–water interface.[94,95] Two hours after addition, a single layer of bubbles had accumulated around the edge of the tank covering ~ 10–15% of the surface. This decreased to $\sim 5\%$ a day later and disappeared after three days, presumably due to the consumption of the BSA by the heterotrophic community (Fig. S6†), by which time the aerosol and INP emissions were rebounding (Fig. 5).

The BSA monolayer will most likely have inhibited INP emissions in two ways. Firstly, it will have displaced the pre-existing SML and the INEs enriched within it. Secondly, it changed bubble bursting behaviour in a way that dampened emissions in general. Bubble bursting produces both film drops, from the disintegration of the thin bubble film, and jet drops, from the breakup of the water jet formed by the collapse of the bubble cavity. Larger bubbles with a radius ≥1 mm generate mainly film drops when the cap disintegrates. Film drops produce SSA with a broad range of sizes and a dry diameter mode at approximately 0.1 μm,[43] as indicated in Fig. 5b. By contrast, bubbles <0.5 mm radius produce only jet drops,[96,97] which are larger than film drops with a dry SSA mode

980 | *Environ. Sci.: Atmos.*, 2023, **3**, 970–990

© 2023 The Author(s). Published by the Royal Society of Chemistry
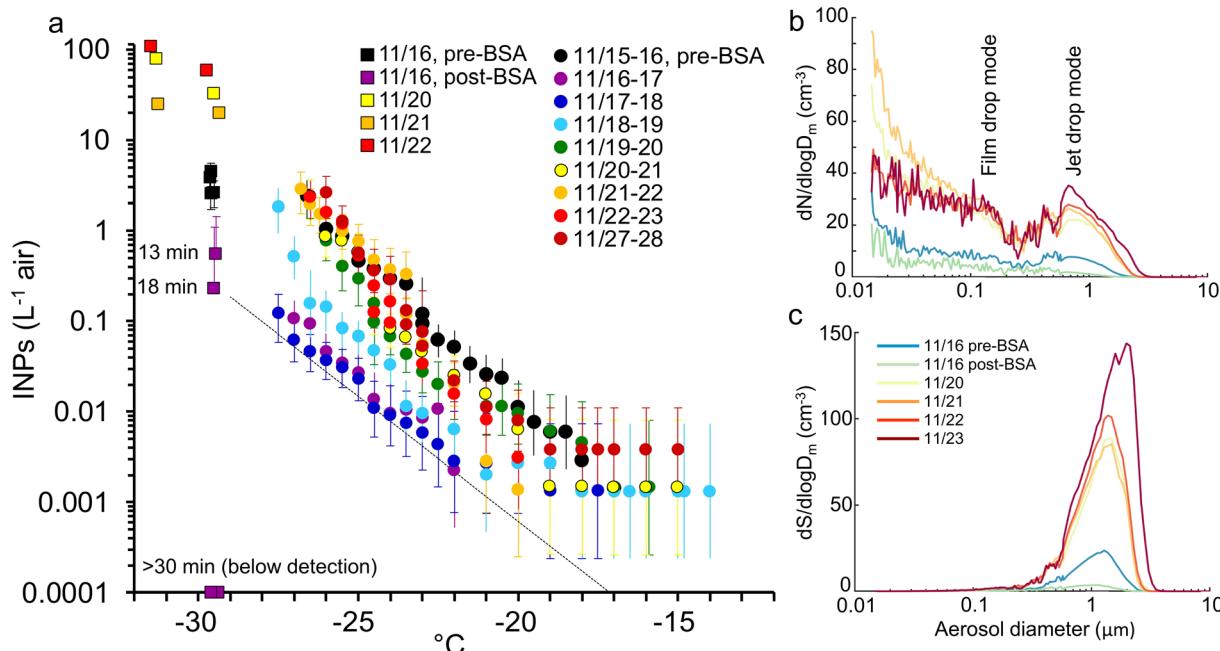
Fig. 5 a) INP spectra in the SSA measured with the ice spectrometer (circles) and the Continuous Flow Diffusion Chamber (squares) during the BSA + sugars addition experiment. The dashed line shows the estimated background INP level on filters. Numbers beside CFDC symbols show time after the addition of BSA + sugars. (b and c) aerosol emissions (dry) over the course of the experiment expressed on the basis of number and surface area, respectively. The post-BSA measures are the average of three scans taken 10–30 min after BSA addition.

at ~0.7 μm (Fig. 5b). Since the diameter of a dry SSA particle is ~$\frac{1}{4}$ of the diameter of its parent droplet,[98] this equates to a fresh jet drop mode diameter of ~3 μm. Further, the radius of the original bubble is ~20× the diameter of the dry SSA particle produced by the top jet drop,[43,96,97,99] which translates to a bubble radius of ~14 μm. The mode is comparable with the maximal production of bubbles of 20–40 μm radius generated in the miniMART with fresh seawater.[45]

Addition of BSA reduced film drop emissions, but especially diminished jet drop emissions (Fig. 5b and c). Modini *et al.* (2013)[100] observed a similar quenching (79–98%) of aerosol production following the addition of a surfactant, Triton X-100, and ascribed several mechanisms to the reduction: the surfactant increased bubble longevity allowing films to drain and thin out before breaking, while the reduced surface tension caused a less explosive contraction of the film upon rupture. Both actions reduced the production of SSA upon film disintegration. Due to the reduction in surface tension, surfactants also reduce the jet height, speed and width, and, hence, the number of jet drops released.[101] The formation of stable islands of bubbles will also have reduced jet drop production.

Jet drops accounted for the bulk of the surface area and volume of emissions before BSA addition. They may also be enriched in INEs due to organic particles adsorbing to the outside of bubbles combined with boundary layer flow concentrating these organics at the bubble bases through which the jet drops erupt.[43,102,103] Hence, a strong quenching of jet drop production by BSA likely caused the collapse in INP emissions.[43] Finally, it is possible that the BSA bound directly to the INEs, forming flocs too large to be ejected.

3.4 Controls over INP emissions

The previous experiments have shown that changes in INP emissions over the incubations may be distilled into the following equation:

$$\Delta INP_{SSA} = \Delta INE_{water} \times \Delta INE_{SML} \times \Delta SSA$$

where each component is the fractional change, from left to right in: INPs in the SSA, INEs present in the bulk water, INE enrichment in the SML, and overall SSA emissions (total particle number, surface area or volume, with changes in SSA driven by changes in SML composition modifying jet drop emissions). INEs in this relationship are limited to those small enough to be ejected inside jet drops; it does not, therefore, include INEs enmeshed within large microgels, macrogels and transparent exopolymer particles.[75,104]

We can use the *P. marinus* addition experiment to attempt to apportion these controls over production and release of INPs in nascent sea spray. Upon addition of dead *P. marinus* detritus, aerosol emissions initially decreased modestly (Fig. 6a), but then over the following days rebounded, reaching a peak 4 days later. The initial suppression followed by the progressive increase in across-the-board particle emissions suggests that an SML with surfactant properties initially formed from the release of material in the added detritus, inhibiting film and especially jet drop emissions (Fig. 6b) just as occurred with BSA. Presumably, this SML was then consumed by the heterotrophic bacteria or progressively removed by continuous SSA production. Interestingly, Christiansen *et al.* (2019)[105] also observed a reduction in SSA number concentration with increasing

© 2023 The Author(s). Published by the Royal Society of Chemistry

Environ. Sci.: Atmos., 2023, **3**, 970–990 | **981**
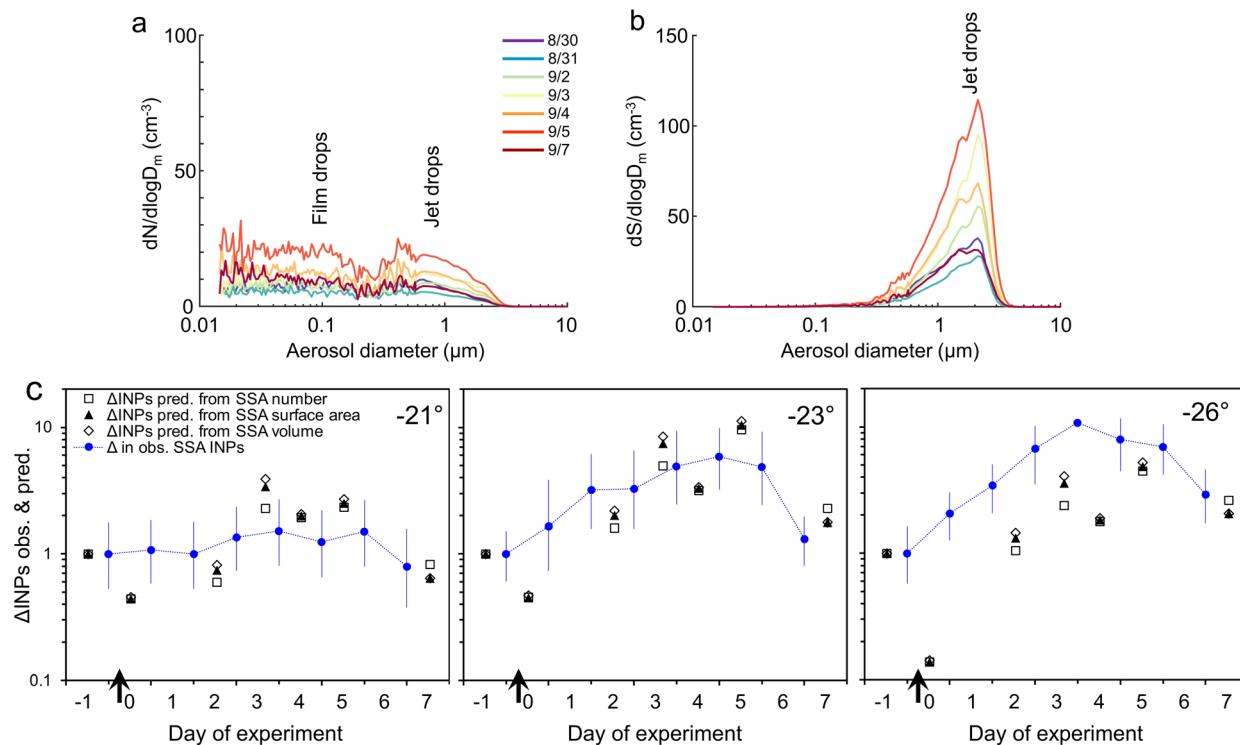
Fig. 6 Aerosol emissions over the course of the *P. marinus* addition experiment expressed on the basis of number (a) and surface area (b). (c) Observed changes in SSA INPs during the *P. marinus* experiment, expressed as the ratio of INPs on Day *x* with the value at the start (before the addition of detritus) compared with changes in SSA INPs predicted from ΔINEs in the water × ΔSSA emissions (given on the bases of aerosol number, surface area and volume).

additions of previously frozen *S. marinoi* cells to a tank using plunging jets to generate SSA.

If we assume (for the sake of this exercise) that level of INE enrichment in the SML was constant, we can use the relative changes (value on Day *x*/value at the start) in the other two terms to predict INPs in the aerosol (Fig. 6c). For SSA INPs active at −21 and −23 °C there is good correspondence between observed and predicted values. However, at −26 °C the observed SSA INP concentration is generally, although improving later in the incubation, several times higher than predicted, presumably due to higher enrichment of INEs active at this temperature in the SML. (No consistent improvement is seen when SSA volume is used in place of surface area to predict INPs, as suggested by Mitts *et al.* (2021).[40]) Bacteria are typically enriched >10-fold in the SML,[91,92] partly due their association with gels.[91] Amino acids and protein-like substances also accumulate in the SML.[78,106] Up to ∼10-fold enrichment of INEs in the SML is commonly observed in mesocosm experiments,[25,107] as well as in field samples.[22,24,30,35,108,109]

Data from the *P. marinus* addition experiment can also be used to estimate the enrichment of INPs in the SSA relative to the bulk water. INPs per volume of freshly-emitted SSA were derived from the integrated volume of dry SSA. Dry SSA diameters were scaled up to obtain total droplet volume by assuming 4× the dry SSA particle diameter represented the diameter of the fresh drop.[98] INPs in the SSA were thus converted to INPs per mL of fresh sea spray, and this was divided by the INEs

per mL of bulk water to obtain enrichment factors ($EF_{Bulk \rightarrow SSA}$) (Fig. 7). At the start, before inoculum addition, the $EF_{Bulk \rightarrow SSA}$ values at all INP temperatures were 160–280. After inoculum addition, the $EF_{Bulk \rightarrow SSA}$ increased several-fold and tended to be higher for colder INPs.

These estimated enrichment factors correspond to values found in previous studies of SSA organics, which often range from ∼100- to >10 000-fold,[91,104,110–112] although they can be higher for lipids, proteins and carbohydrates.[93,113,114] Organic matter in submicron particles is almost entirely water insoluble
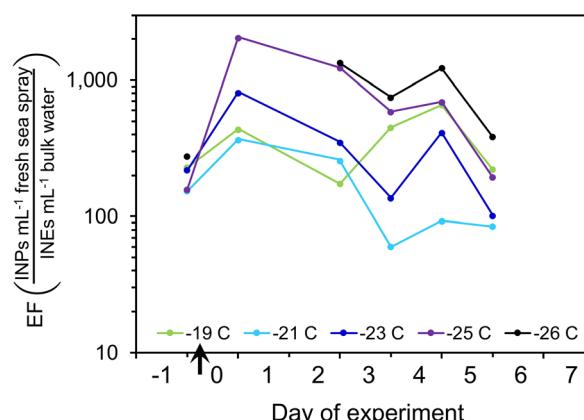
Fig. 7 Enrichment factors for INPs active at different temperatures over the course of the *P. marinus* addition experiment.

and was found to consist of colloids and aggregates exuded by phytoplankton,[115] whereas Bio (*i.e.*, protein and phosphate-containing) particles were dominant at sizes >1 μm.[68,116]

4 Conclusions

When phytoplankton blooms collapse, the ensuing decomposer community of bacteria, and the viruses and grazers that prey upon them, comminute, consume and transform the biomass. The constituents and/or by-products of this community consistently possess ice nucleation activity.[3,25,39,40] To test if INE production depends upon phytoplankton type we added dead POC biomass of a green alga (*N. atomus*), a diatom (*S. marinoi*) and a cyanobacterium (*P. marinus*) to a miniMART filled with fresh seawater. Over the next two days, heterotrophic bacteria concentrations increased then plateaued, and after several more days decreased, coincident with an increase in HNF and, in two cases, viruses. Enzyme activities typically increased over the first few days, while HULIS steadily accumulated.

INEs in the water initially decreased or remained stable, but after 1–4 days they rebounded, increasing by up to 18-, 14- and 7-fold in the *N. atomus*, *S. marinoi*, and *P. marinus* incubations, respectively. Newly fabricated INEs were organic, mostly not heat labile, and varied in size (all <0.2, a mix of sizes, or all >0.2 μm). INE concentration active at −23 °C was closely correlated with HNF, and also with viruses and the concentration of HULIS, but not with heterotrophic bacteria concentrations. Sources of INEs may thus include:

• Components of the new populations of HNF and/or viruses, and/or debris of bacteria consumed by HNF and viruses.

  • Newly-formed HULIS.

  • Progressive fragmentation of INEs or release of IN-monolayers composed of fatty alcohols/acids and possible crystallites of these[117,118] from the consumed bacteria or phytoplankton.

Changes in emissions of INPs in the SSA generally paralleled those in the water, but tended to peak a day or so earlier. The most pronounced increases occurred with the diatom *S. marinoi* (up to 35-fold higher) and cyanobacterium *P. marinus* (up to 15-fold higher) incubations. Several mechanisms could explain the early peak in INP emissions: (1) initially-formed INEs had characteristics that led to their greater enrichment in the SML than those produced later, (2) progressive enmeshment of INEs within larger gels reduced their emissions after a few days, (3) changes in the SML may have altered INE emissions by altering enrichment and/or changing surface tension and bubble longevity. We should note that in the ocean algae are often nutrient depleted and the bacterial degradation of algal detritus may create a different molecular fingerprint, affecting INE emissions differently than observed here. Hence, it would be premature to extrapolate from this and similar studies to estimate INE production *in situ*.

Sequencing of bacteria in the *N. atomus* addition experiment showed three groups, known to dominate bloom-associated bacterial communities, comprising ~95% of the abundant OTUs at the peak of INP production. Several OTUs greatly increased their relative abundances in both the water and SSA over the peak period of INPs emissions, although none are currently associated with known groups of ice nucleation-active bacteria.

To test if INE production is simply the result of an injection of nutrients, we added a simple DOC cocktail (BSA + three monosaccharides) to a fourth incubation. INE concentrations in the water remained essentially unchanged. Unexpectedly, INP emissions in the SSA abruptly fell due to the formation of a BSA monolayer, which will have displaced the pre-existing SML and INEs enriched within it, and altered bubble bursting behaviour, in particular, by reducing jet drop emissions. Since jet drops accounted for the bulk of the surface area and volume of the SSA, their quenching effectively shut down INP emissions. This serendipitous result revealed the strong control of the SML over INP emissions, directly *via* INP enrichment and indirectly *via* bubble bursting.

Overall, changes in INP emissions are the complex product of (1) changes of INPs in the water, (2) INE enrichment in the SML, and (3) SSA emissions, due to altered SML composition modifying jet drop production. From the *P. marinus* incubation we estimate that INP enrichment in the SSA was around 160–280 for fresh seawater, and likely increases during the decay phase of the phytoplankton bloom. We believe this is the first estimate of $EF_{Bulk \to SSA}$ for marine INPs.

Collectively, these experiments revealed that the production of INEs following the collapse of phytoplankton blooms requires a heterogeneous substrate to initiate a complex natural succession of decomposers. INP emissions are enhanced by INE enrichment in the SML and enhanced or reduced by the SML's influence over jet drop production.

If phytoplankton blooms consistently generate and emit INPs, their atmospheric contribution would be most pronounced in remote regions of the SO.[2] Chl *a* concentrations range widely (annual mean >0.1 to >2 mg m^{-3}) across the SO,[119] with a timing, scale, and biomass varying latitudinally and regionally. Latitudinally, blooms are driven by sunlight: in temperate "bioregions", phytoplankton blooms occur in October, whereas near Antarctica they peak in January/February.[119] In regions where currents interact with continental shelves, islands and hydrothermal vents, large blooms develop every spring and summer, fertilized by upwelling of nutrients, especially iron and silicate.[120,121] Some marine and phytoplankton bloom-induced INEs/INPs can possess activity at the exceptionally warm temperatures required for secondary ice multiplication,[22,36,39,108] a process that can generate ice particle concentrations orders of magnitude higher than the numbers of INPs present.

Author contributions

FM, TH, CM, GS, PD and KP designed the study. GC, CL and MS collected and shipped the seawater samples. TH and AR performed the INP measurements. RP automated the Ice Spectrometer. CM, GS, EL and KS operated the CFDC, while GS and KM processed the CFDC results. TH prepared filters and took the INP samples, and also performed the DNA extractions. FM

prepared the phytoplankton biomass, and performed the collection and analysis of microbial counts and enzyme activities. MS provided the EEM analyses. PDN provided the Skeletonema culture. KM, GS and CM analysed the aerosol sizing data and merged the distributions. TH, FM, KM, CM, MS, PD, RP and MC contributed significantly to the analyses and presentation of figures. All authors contributed to the writing and editing of the article.

Conflicts of interest

There are no conflicts to declare.

Acknowledgements

References

1 J. Uetake, T. C. J. Hill, K. A. Moore, P. J. DeMott, A. Protat and S. M. Kreidenweis, Airborne bacteria confirm the pristine nature of the Southern Ocean boundary layer, *Proc. Natl. Acad. Sci. U.S.A.*, 2020, **117**, 13275–13282, DOI: 10.1073/pnas.2000134117.

2 S. M. Burrows, C. Hoose, U. Pöschl and M. G. Lawrence, Ice nuclei in marine air: Biogenic particles or dust?, *Atmos. Chem. Phys.*, 2013, **13**, 245–267, DOI: 10.5194/acp-13-245-2013.

3 P. J. DeMott, T. C. J. Hill, C. S. McCluskey, K. A. Prather, D. B. Collins, R. C. Sullivan, M. J. Ruppel, R. H. Mason, V. E. Irish, T. Lee, C. Y. Hwang, T. S. Rhee, J. R. Snider, G. R. McMeeking, S. Dhaniyala, E. R. Lewis, J. J. B. Wentzell, J. Abbatt, C. Lee, C. M. Sultana, A. P. Ault, J. L. Axson, M. Diaz Martinez, I. Venero, G. Santos-Figueroa, M. D. Stokes, G. B. Deane, O. L. Mayol-Bracero, V. H. Grassian, T. H. Bertram, A. K. Bertram, B. F. Moffett and G. D. Franc, Sea spray aerosol as a unique source of ice nucleating particles, *Proc. Natl. Acad. Sci. U.S.A.*, 2016, **113**, 5797–5803, DOI: 10.1073/pnas.1514034112.

4 G. M. McFarquhar, C. S. Bretherton, R. Marchand, A. Protat, P. J. DeMott, S. P. Alexander, G. C. Roberts, C. H. Twohy, D. Toohey, S. Siems, Y. Huang, R. Wood, R. M. Rauber, S. Lasher-Trapp, J. Jensen, J. L. Stith, J. Mace, J. Um, E. Järvinen, M. Schnaiter, A. Gettelman, K. J. Sanchez, C. S. McCluskey, L. M. Russell, I. L. McCoy, R. L. Atlas, C. G. Bardeen, K. A. Moore, T. C. J. Hill, R. S. Humphries, M. D. Keywood, Z. Ristovski, L. Cravigan, R. Schofield, C. Fairall, M. D. Mallet, S. M. Kreidenweis, B. Rainwater,

J. D'Alessandro, Y. Wang, W. Wu, G. Saliba, E. J. T. Levin, S. Ding, F. Lang, S. C. H. Truong, C. Wolff, J. Haggerty, M. J. Harvey, A. R. Klekociuk and A. McDonald, Observations of clouds, aerosols, precipitation, and surface radiation over the Southern Ocean: An overview of Capricorn, Marcus, Micre, and Socrates, *Bull. Am. Meteorol. Soc.*, 2021, **102**, E894–E928, DOI: 10.1175/BAMS-D-20-0132.1.

5 Y.-T. Hwang and D. M. W. Frierson, A link between the double-Intertropical Convergence Zone problem and cloud biases over the Southern Ocean, *Proc. Natl. Acad. Sci. U.S.A.*, 2013, **110**, 4935–4940, DOI: 10.1073/pnas.1213302110.

6 J. E. Kay, C. Wall, V. Yettella, B. Medeiros, C. Hannay, P. Caldwell and C. Bitz, Global climate impacts of fixing the Southern Ocean shortwave radiation bias in the Community Earth System Model (CESM), *J. Clim.*, 2016, **29**, 4617–4636, DOI: 10.1175/JCLI-D-15-0358.1.

7 D. T. McCoy, D. L. Hartmann, M. D. Zelinka, P. Ceppi and D. P. Grosvenor, Mixed-phase cloud physics and Southern Ocean cloud feedback in climate models, *J. Geophys. Res.: Atmos.*, 2015, **120**, 9539–9554, DOI: 10.1002/2015JD023603.

8 I. Tan, T. Storelvmo and M. D. Zelinka, Observational constraints on mixed-phase clouds imply higher climate sensitivity, *Science*, 2016, **352**(6282), 224–227, DOI: 10.1126/science.aad5300.

9 A. Bodas-Salcedo, P. G. Hill, K. Furtado, K. D. Williams, P. R. Field, J. C. Manners, P. Hyder and S. Kato, Large contribution of supercooled liquid clouds to the solar radiation budget of the Southern Ocean, *J. Clim.*, 2016, **29**, 4213–4228, DOI: 10.1175/JCLI-D-15-0564.1.

10 J. Vergara-Temprado, A. K. Miltenberger, K. Furtado, D. P. Grosvenor, B. J. Shipway, A. A. Hill, J. M. Wilkinson, P. R. Field, B. J. Murray and K. S. Carslaw, Strong control of Southern Ocean cloud reflectivity by ice-nucleating particles, *Proc. Natl. Acad. Sci. U.S.A.*, 2018, **115**, 2687–2692, DOI: 10.1073/pnas.1721627115.

11 É. Vignon, S. P. Alexander, P. J. DeMott, G. Sotiropoulou, F. Gerber, T. C. J. Hill, R. Marchand, A. Nenes and A. Berne, Challenging and improving the simulation of mid-level mixed-phase clouds over the high-latitude Southern Ocean, *J. Geophys. Res.: Atmos.*, 2021, **126**, e2020JD033490, DOI: 10.1029/2020JD033490.

12 K. E. Trenberth and J. T. Fasullo, Simulation of present-day and twenty-first-century energy budgets of the southern oceans, *J. Climatol.*, 2010, **23**, 440–454, DOI: 10.1175/2009JCLI3152.1.

13 T. J. Zaremba, R. M. Rauber, G. M. McFarquhar, M. Hayman, J. A. Finlon and D. M. Stechman, Phase characterization of cold sector Southern Ocean cloud tops: results from Socrates, *J. Geophys. Res.: Atmos.*, 2020, **125**, e2020JD033673, DOI: 10.1029/2020JD033673.

14 S. Kremser, M. Harvey, P. Kuma, S. Hartery, A. Saint-Macary, J. McGregor, A. Schuddeboom, M. von Hobe, S. T. Lennartz, A. Geddes, R. Querel, A. McDonald, M. Peltola, K. Sellegri, I. Silber, C. S. Law, C. J. Flynn, A. Marriner, T. C. J. Hill, P. J. DeMott, C. C. Hume,

G. Plank, G. Graham and S. Parsons, Southern Ocean Cloud and Aerosol data: a compilation of measurements from the 2018 Southern Ocean Ross Sea Marine Ecosystems and Environment voyage, *Earth Syst. Sci. Data*, 2021, **13**, 3115–3153, DOI: **10.5194/essd-13-3115-2021**.

15 C. S. McCluskey, J. Ovadnevaite, M. Rinaldi, J. Atkinson, F. Belosi, D. Ceburnis, M. Salvatore, T. C. J. Hill, U. Lohmann, Z. A. Kanji, C. O'Dowd, S. M. Kreidenweis and P. J. DeMott, Marine and terrestrial organic ice-nucleating particles in pristine marine to continentally influenced Northeast Atlantic air masses, *J. Geophys. Res.: Atmos.*, 2018, **123**, 6196–6212, DOI: **10.1029/2017JD028033**.

16 A. Welti, E. K. Bigg, P. J. DeMott, X. Gong, M. Hartmann, M. Harvey, S. Henning, P. Herenz, T. C. J. Hill, B. Hornblow, C. Leck, M. Löffler, C. S. McCluskey, A. M. Rauker, J. Schmale, C. Tatzelt, M. van Pinxteren and F. Stratmann, Ship-based measurements of ice nuclei concentrations over the Arctic, Atlantic, Pacific and Southern oceans, *Atmos. Chem. Phys.*, 2020, **20**, 15191–15206, DOI: **10.5194/acp-20-15191-2020**.

17 M. D. Zelinka, T. A. Myers, D. T. McCoy, S. Po-Chedley, P. M. Caldwell, P. Ceppi, S. A. Klein and K. E. Taylor, Causes of higher climate sensitivity in CMIP6 models, *Geophys. Res. Lett.*, 2020, **47**, e2019GL085782, DOI: **10.1029/2019GL085782**.

18 A. Gettelman, C. G. Bardeen, C. S. McCluskey, E. Järvinen, J. Stith, C. Bretherton, G. McFarquhar, C. Twohy, J. D'Alessandro and W. Wu, Simulating observations of Southern Ocean clouds and implications for climate, *J. Geophys. Res.: Atmos.*, 2020, **125**, e2020JD032619, DOI: **10.1029/2020JD032619**.

19 W. T. K. Huang, L. Ickes, I. Tegen, M. Rinaldi, D. Ceburnis and U. Lohmann, Global relevance of marine organic aerosol as ice nucleating particles, *Atmos. Chem. Phys.*, 2018, **18**, 11423–11445, DOI: **10.5194/acp-18-11423-2018**.

20 X. Zhao, X. Liu, S. M. Burrows and Y. Shi, Effects of marine organic aerosols as sources of immersion-mode ice-nucleating particles on high-latitude mixed-phase clouds, *Atmos. Chem. Phys.*, 2021, **21**, 2305–2327, DOI: **10.5194/acp-21-2305-2021**.

21 T. Raatikainen, M. Prank, J. Ahola, H. Kokkola, J. Tonttila and S. Romakkaniemi, The effect of marine ice-nucleating particles on mixed-phase clouds, *Atmos. Chem. Phys.*, 2022, **22**, 3763–3778, DOI: **10.5194/acp-22-3763-2022**.

22 M. Hartmann, X. Gong, S. Kecorius, M. van Pinxteren, T. Vogl, A. Welti, H. Wex, S. Zeppenfeld, H. Herrmann, A. Wiedensohler and F. Stratmann, Terrestrial or marine–indications towards the origin of ice-nucleating particles during melt season in the European Arctic up to 83.7°N, *Atmos. Chem. Phys.*, 2021, **21**, 1613–11636, DOI: **10.5194/acp-21-11613-2021**.

23 V. E. Irish, P. Elizondo, J. Chen, C. Chou, J. Charette, M. Lizotte, L. A. Ladino, T. W. Wilson, M. Gosselin, B. J. Murray and E. Polishchuk, Ice-nucleating particles in Canadian Arctic sea-surface microlayer and bulk seawater, *Atmos. Chem. Phys.*, 2017, **17**, 10583–10595, DOI: **10.5194/acp-17-10583-2017**.

24 V. E. Irish, S. J. Hanna, X. Yu, M. Boyer, E. Polishchuk, M. Ahmed, J. Chen, J. P. Abbatt, M. Gosselin, R. Chang, L. A. Miller and A. K. Bertram, Revisiting properties and concentrations of ice-nucleating particles in the sea surface microlayer and bulk seawater in the Canadian Arctic during summer, *Atmos. Chem. Phys.*, 2019, **19**, 7775–7787, DOI: **10.5194/acp-19-7775-2019**.

25 C. S. McCluskey, T. C. J. Hill, C. M. Sultana, O. Laskina, J. Trueblood, M. V. Santander, C. M. Beall, J. M. Michaud, S. M. Kreidenweis, K. A. Prather, V. H. Grassian and P. J. DeMott, A mesocosm double feature: Insights into the chemical make-up of marine ice nucleating particles, *J. Atmos. Sci.*, 2018, **75**, 2405–2423, DOI: **10.1175/JAS-D-17-0155.1**.

26 B. F. Moffett, Fresh water ice nuclei, *Fundam. Appl. Limnol.*, 2016, **188**, 19–23, DOI: **10.1127/fal/2016/0851**.

27 J. Rosinski, P. L. Haagenson, C. T. Nagamoto, B. Quintana, F. Parungo and S. D. Hoyt, Ice-forming nuclei in air masses over the Gulf of Mexico, *J. Aerosol Sci.*, 1988, **19**, 539–551, DOI: **10.1016/0021-8502(88)90206-6**.

28 R. Schnell, Ice nuclei in seawater, fog water and marine air off the Coast of Nova Scotia: summer 1975, *J. Atmos. Sci.*, 1977, **34**, 1299–1305, DOI: **10.1175/1520-0469(1977)034%3C1299:INISFW%3E2.0.CO;2**.

29 R. C. Schnell and G. Vali, Freezing nuclei in marine waters, *Tellus*, 1975, **27**, 321–323, DOI: **10.1111/j.2153-3490.1975.tb01682.x**.

30 T. W. Wilson, L. A. Ladino, P. A. Alpert, M. N. Breckels, I. M. Brooks, J. Browse, S. M. Burrows, K. S. Carslaw, J. A. Huffman, C. Judd, W. P. Kilthau, R. H. Mason, G. McFiggans, L. A. Miller, J. J. Nájera, E. Polishchuk, S. Rae, C. L. Schiller, M. Si, J. V. Temprado, T. F. Whale, J. P. S. Wong, O. Wurl, J. D. Yakobi-Hancock, J. P. D. Abbatt, J. Y. Aller, A. K. Bertram, D. A. Knopf and B. J. Murray, A marine biogenic source of atmospheric ice-nucleating particles, *Nature*, 2015, **525**, 234–238, DOI: **10.1038/nature14986**.

31 T. C. J. Hill, P. J. DeMott, Y. Tobo, J. Fröhlich-Nowoisky, B. F. Moffett, G. D. Franc and S. M. Kreidenweis, Sources of organic ice nucleating particles in soils, *Atmos. Chem. Phys.*, 2016, **16**, 7195–7721, DOI: **10.5194/acp-16-7195-2016**.

32 Z. A. Kanji, L. A. Ladino, H. Wex, Y. Boose, M. Burkert-Kohn, D. J. Cziczo and M. Krämer, Overview of ice nucleating particles, *Meteorol. Monogr.*, 2017, **58**, 1.1–1.33, DOI: **10.1175/AMSMONOGRAPHS-D-16-0006.1**.

33 E. K. Bigg, Ice nucleus measurements in remote areas, *J. Atmos. Sci.*, 1973, **30**, 1153–1157.

34 C. S. McCluskey, T. C. J. Hill, R. S. Humphries, A. M. Rauker, S. Moreau, P. G. Strutton, S. D. Chambers, A. G. Williams, I. McRobert, J. Ward, M. D. Keywood, J. Harnwell, W. Ponsonby, Z. M. Loh, P. B. Krummel, A. Protat, S. M. Kreidenweis and P. J. DeMott, Observations of ice nucleating particles over Southern Ocean waters, *Geophys. Res. Lett.*, 2018, **45**, 11989–11997, DOI: **10.1029/2018GL079981**.

35 J. V. Trueblood, A. Nicosia, A. Engel, B. Zäncker, M. Rinaldi, E. Freney, M. Thyssen, I. Obernosterer, J. Dinasquet,

© 2023 The Author(s). Published by the Royal Society of Chemistry

Environ. Sci.: Atmos., 2023, **3**, 970–990 | **985**

F. Belosi and A. Tovar-Sánchez, A two-component parameterization of marine ice-nucleating particles based on seawater biology and sea spray aerosol measurements in the Mediterranean Sea, *Atmos. Chem. Phys.*, 2021, **21**, 4659–4676, DOI: **10.5194/acp-21-4659-2021**.

36 R. C. Schnell and G. Vali, Biogenic ice nuclei: part I. Terrestrial and marine sources, *J. Atmos. Sci.*, 1976, **33**, 1554–1564, DOI: **10.1175/1520-0469(1976)033%3C1554:BINPIT%3E2.0.CO;2**.

37 J. Rosinski, P. L. Haagenson, C. T. Nagamoto and F. Parungo, Ice-forming nuclei of maritime origin, *J. Aerosol Sci.*, 1986, **17**, 23–46, DOI: **10.1016/0021-8502(86)90004-2**.

38 J. M. Creamean, J. N. Cross, R. Pickart, L. McRaven, P. Lin, A. Pacini, R. Hanlon, D. G. Schmale, J. Ceniceros, T. Aydell, N. Colombi, E. Bolger and P. J. DeMott, Ice nucleating particles carried from below a phytoplankton bloom to the Arctic atmosphere, *Geophys. Res. Lett.*, 2019, **46**, 8572–8581, DOI: **10.1029/2019GL083039**.

39 C. S. McCluskey, T. C. J. Hill, F. Malfatti, C. M. Sultana, C. Lee, M. V. Santander, C. M. Beall, K. A. Moore, G. C. Cornwell, D. B. Collins, K. A. Prather, T. Jayarathne, E. A. Stone, F. Azam, S. M. Kreidenweis and P. J. DeMott, A dynamic link between ice nucleating particles released in nascent sea spray aerosol and oceanic biological activity during two mesocosm experiments, *J. Atmos. Sci.*, 2017, **74**, 151–166, DOI: **10.1175/JAS-D-16-0087.1**.

40 B. A. Mitts, X. Wang, D. D. Lucero, C. M. Beall, G. B. Deane, P. J. DeMott and K. A. Prather, Importance of supermicron ice nucleating particles in nascent sea spray, *Geophys. Res. Lett.*, 2021, **48**, e2020GL089633, DOI: **10.1029/2020GL089633**.

41 X. Wang, C. M. Sultana, J. Trueblood, T. C. J. Hill, F. Malfatti, C. Lee, O. Laskina, K. A. Moore, C. M. Beall, C. S. McCluskey, G. C. Cornwell, Y. Zhou, J. L. Cox, M. A. Pendergraft, M. V. Santander, T. H. Bertram, C. D. Cappa, F. Azam, P. J. DeMott, V. H. Grassian and K. A. Prather, Microbial control of sea spray aerosol composition: A tale of two blooms, *ACS Cent. Sci.*, 2015, **1**, 124–131, DOI: **10.1021/acscentsci.5b00148**.

42 L. Ickes, G. C. Porter, R. Wagner, M. P. Adams, S. Bierbauer, A. K. Bertram, M. Bilde, S. Christiansen, A. M. Ekman, E. Gorokhova, K. Höhler, A. A. Kiselev, C. Leck, O. Möhler, B. J. Murray, T. Schiebel, R. Ullrich and M. E. Salter, The ice-nucleating activity of Arctic sea surface microlayer samples and marine algal cultures, *Atmos. Chem. Phys.*, 2020, **20**, 11089–11117, DOI: **10.5194/acp-20-11089-2020**.

43 X. Wang, G. B. Deane, K. A. Moore, O. S. Ryder, M. D. Stokes, C. M. Beall, D. B. Collins, M. V. Santander, S. M. Burrows, C. M. Sultana and K. A. Prather, The role of jet and film drops in controlling the mixing state of submicron sea spray aerosol particles, *Proc. Natl. Acad. Sci. U.S.A.*, 2017, **114**, 6978–6983, DOI: **10.1073/pnas.1702420114**.

44 G. C. Cornwell, C. M. Sultana, M. Prank, R. E. Cochran, T. C. Hill, G. P. Schill, P. J. DeMott, N. Mahowald and K. A. Prather, Ejection of dust from the ocean as a potential source of marine ice nucleating particles, *J. Geophys. Res.: Atmos.*, 2020, e2020JD033073, DOI: **10.1029/2020JD033073**.

45 M. D. Stokes, G. Deane, D. B. Collins, C. Cappa, T. Bertram, A. Dommer, S. Schill, S. Forestieri and M. Survilo, A miniature Marine Aerosol Reference Tank (miniMART) as a compact breaking wave analogue, *Atmos. Meas. Tech.*, 2016, **9**, 4257–4267, DOI: **10.5194/amt-9-4257-2016**.

46 J. W. Ammerman, J. A. Fuhrman, A. Hagström and F. Azam, Bacterioplankton growth in seawater: I. Growth kinetics and cellular characteristics in seawater cultures, *Mar. Ecol. Prog. Ser.*, 1984, **18**, 31–39, DOI: **10.3354/meps018031**.

47 K. D. Bidle and F. Azam, Accelerated dissolution of diatom silica by marine bacterial assemblages, *Nature*, 1999, **397**(6719), 508–512, DOI: **10.1038/17351**.

48 O. Holm-Hansen and B. Riemann, Chlorophyll a determination: improvements in methodology, *Oikos*, 1978, **30**, 438–447, DOI: **10.2307/3543338**.

49 L. A. Ladino, J. D. Yakobi-Hancock, W. P. Kilthau, R. H. Mason, M. Si, J. Li, L. A. Miller, C. L. Schiller, J. A. Huffman, J. Y. Aller, D. A. Knopf, A. K. Bertram and J. P. D. Abbatt, Addressing the ice nucleating abilities of marine aerosol: A combination of deposition mode laboratory and field measurements, *Atmos. Environ.*, 2016, **132**, 1–10, DOI: **10.1016/j.atmosenv.2016.02.028**.

50 P. A. Alpert, J. Y. Aller and D. A. Knopf, Initiation of the ice phase by marine biogenic surfaces in supersaturated gas and supercooled aqueous phases, *Phys. Chem. Chem. Phys.*, 2011, **13**, 19882–19894, DOI: **10.1039/C1CP21844A**.

51 Y. Xi, A. Mercier, C. Kuang, J. Yun, A. Christy, L. Melo, M. T. Maldonado, J. A. Raymond and A. K. Bertram, Concentrations and properties of ice nucleating substances in exudates from Antarctic sea-ice diatoms, *Environ. Sci.: Processes Impacts*, 2021, **23**, 323–334, DOI: **10.1039/d0em00398k**.

52 J. M. Michaud, L. R. Thompson, D. Kaul, J. L. Espinoza, R. A. Richter, Z. Z. Xu, C. Lee, K. M. Pham, C. M. Beall, F. Malfatti, F. Azam, R. Knight, M. D. Burkart, C. L. Dupont and K. A. Prather, Taxon-specific aerosolization of bacteria and viruses in an experimental ocean-atmosphere mesocosm, *Nat. Commun.*, 2018, **9**(1), 1–10, DOI: **10.1038/s41467-018-04409-z**.

53 R. Benner, J. D. Pakulski, M. McCarthy, J. I. Hedges and P. G. Hatcher, Bulk chemical characteristics of dissolved organic matter in the ocean, *Science*, 1992, **255**, 1561–1564, DOI: **10.1126/science.255.5051.1561**.

54 R. R. L. Guillard, Culture of phytoplankton for feeding marine invertebrates, in *Culture of Marine Invertebrate Animals*, ed. W. L., Smith and M. H., Chanley, Springer, Boston, MA, 1975, pp. 29–60, DOI: **10.1007/978-1-4615-8714-9**.

55 L. R. Moore, A. F. Post, G. Rocap and S. W. Chisholm, Utilization of different nitrogen sources by the marine cyanobacteria Prochlorococcus and Synechococcus, *Limnol. Oceanogr.*, 2002, **47**, 989–996, DOI: **10.4319/lo.2002.47.4.0989**.

56 U. Christaki, C. Courties, R. Massana, P. Catala, P. Lebaron, J. M. Gasol and M. V. Zubkov, Optimized routine flow cytometric enumeration of heterotrophic flagellates using SYBR Green I, *Limnol. Oceanogr. Methods*, 2011, **9**, 329–339, DOI: **10.4319/lom.2011.9.329**.

57 J. M. Gasol and P. A. Del Giorgio, Using flow cytometry for counting natural planktonic bacteria and understanding the structure of planktonic bacterial communities, *Sci. Mar.*, 2000, **64**, 197–224, DOI: **10.3989/scimar.2000.64n2197**.

58 D. Marie, F. Partensky, S. Jacquet and D. Vaulot, Enumeration and cell cycle analysis of natural populations of marine picoplankton by flow cytometry using the nucleic acid stain SYBR Green I, *Appl. Environ. Microbiol.*, 1997, **63**, 186–193, DOI: **10.1128/aem.63.1.186-193.1997**.

59 R. T. Noble and J. A. Fuhrman, Use of SYBR Green I for rapid epifluorescence counts of marine viruses and bacteria, *Aquat. Microb. Ecol.*, 1998, **14**, 113–118, DOI: **10.3354/ame014113**.

60 H. G. Hoppe, Significance of exoenzymatic activities in the ecology of brackish water: measurements by means of methylumbelliferyl-substrates, *Mar. Ecol. Prog. Ser.*, 1983, **11**, 299–311, DOI: **10.3354/meps011299**.

61 F. Malfatti, C. Lee, T. Tinta, M. A. Pendergraft, M. Celussi, Y. Zhou, C. M. Sultana, A. Rotter, J. L. Axson, D. B. Collins, M. V. Santander, A. L. Anides Morales, L. I. Aluwihare, N. Riemer, V. H. Grassian, F. Azam and K. A. Prather, Detection of active microbial enzymes in nascent sea spray aerosol: implications for atmospheric chemistry and climate, *Environ. Sci. Technol. Lett.*, 2019, **6**, 171–177, DOI: **10.1021/acs.estlett.8b00699**.

62 J. Martinez, D. C. Smith, D. F. Steward and F. Azam, Variability in ectohydrolytic enzyme activities of pelagic marine bacteria and its significance for substrate processing in the sea, *Aquat. Microb. Ecol.*, 1996, **10**, 223–230, DOI: **10.3354/ame010223**.

63 N. Hiranuma, S. Augustin-Bauditz, H. Bingemer, C. Budke, J. Curtius, A. Danielczok, K. Diehl, K. Dreischmeier, M. Ebert, F. Frank, N. Hoffman, K. Kandler, A. Kiselev, T. Koop, T. Leisner, O. Möhler, B. Nillius, A. Peckhaus, D. Rose, S. Weinbruch, H. Wex, Y. Boose, P. J. DeMott, J. D. Hader, T. C. J. Hill, Z. A. Kanji, G. Kulkarni, E. J. T. Levin, C. S. McCluskey, M. Murakami, B. J. Murray, D. Niedermeier, M. D. Petters, D. O'Sullivan, A. Saito, G. P. Schill, T. Tajiri, M. A. Tolbert, A. Welti, T. F. Whale, T. P. Wright and K. Yamashita, A comprehensive laboratory study on the immersion freezing behavior of illite NX particles: a comparison of 17 ice nucleation measurement techniques, *Atmos. Chem. Phys.*, 2015, **15**, 1–30, DOI: **10.5194/acp-15-2489-2015**.

64 A. Agresti and B. A. Coull, Approximate is better than "exact" for interval estimation of binomial proportions, *Am. Stat.*, 1998, **52**, 119–126, DOI: **10.1080/00031305.1998.10480550**.

65 F. Azam and F. Malfatti, Microbial structuring of marine ecosystems, *Nat. Rev. Microbiol.*, 2007, **5**, 782–791, DOI: **10.1038/nrmicro1747**.

66 D. C. Rogers, P. J. DeMott, S. M. Kreidenweis and Y. Chen, A continuous-flow diffusion chamber for airborne measurements of ice nuclei, *J. Atmos. Oceanic Technol.*, 2001, **18**, 725–741, DOI: **10.1175/1520-0426(2001)018%3C0725:ACFDCF%3E2.0.CO;2**.

67 P. J. DeMott, A. J. Prenni, G. R. McMeeking, R. C. Sullivan, M. D. Petters, Y. Tobo, M. Niemand, O. Möhler, J. R. Snider, Z. Wang and S. M. Kreidenweis, Integrating laboratory and field data to quantify the immersion freezing ice nucleation activity of mineral dust particles, *Atmos. Chem. Phys.*, 2015, **15**, 393–409, DOI: **10.5194/acp-15-393-201**.

68 K. A. Prather, T. H. Bertram, V. H. Grassian, G. B. Deane, M. D. Stokes, P. J. Demott, L. I. Aluwihare, B. P. Palenik, F. Azam, J. H. Seinfeld, R. C. Moffet, M. J. Molina, C. D. Cappa, F. M. Geiger, G. C. Roberts, L. M. Russell, A. P. Ault, J. Baltrusaitis, D. B. Collins, C. E. Corrigan, L. A. Cuadra-Rodriguez, C. J. Ebben, S. D. Forestieri, T. L. Guasco, S. P. Hersey, M. J. Kim, W. F. Lambert, R. L. Modini, W. Mui, B. E. Pedler, M. J. Ruppel, O. S. Ryder, N. G. Schoepp, R. C. Sullivan and D. Zhao, Bringing the ocean into the laboratory to probe the chemical complexity of sea spray aerosol, *Proc. Natl. Acad. Sci. U.S.A.*, 2013, **110**, 7550–7555, DOI: **10.1073/pnas.1300262110**.

69 T. C. J. Hill, D. G. Georgakopoulos, P. J. DeMott, W. L. Stump and G. D. Franc, Measurement of ice nucleation-active bacteria on plants and in precipitation by quantitative PCR, *Appl. Environ. Microbiol.*, 2014, **80**, 1256–1267, DOI: **10.1128/AEM.02967-13**.

70 A. E. Parada, D. M. Needham and J. A. Fuhrman, Every base matters: assessing small subunit rRNA primers for marine microbiomes with mock communities, time series and global field samples, *Environ. Microbiol.*, 2016, **18**, 1403–1414, DOI: **10.1111/1462-2920.13023**.

71 J. R. Cole, Q. Wang, J. A. Fish, B. Chai, D. M. McGarrell, Y. Sun, C. T. Brown, A. Porras-Alfaro, C. R. Kuske and J. M. Tiedje, Ribosomal Database Project: data and tools for high throughput rRNA analysis, *Nucleic Acids Res.*, 2014, **42**, D633–D642, DOI: **10.1093/nar/gkt1244**.

72 T. C. J. Hill, K. A. Walsh, J. A. Harris and B. F. Moffett, Using ecological diversity measures with bacterial communities, *FEMS Microbiol. Ecol.*, 2003, **43**, 1–11, DOI: **10.1111/j.1574-6941.2003.tb01040.x**.

73 A. E. Magurran, *Ecological Diversity and its Measurement*, Chapman and Hall, London, 1988, p. 179, DOI: **10.1007/978-94-015-7358-0**.

74 E. Fuentes, H. Coe, D. Green and G. McFiggans, On the impacts of phytoplankton derived organic matter on the properties of the primary marine aerosol-part 2: composition, hygroscopicity and cloud condensation activity, *Atmos. Chem. Phys.*, 2011, **11**, 2585–2602, DOI: **10.5194/acp-11-2585-2011**.

© 2023 The Author(s). Published by the Royal Society of Chemistry

Environ. Sci.: Atmos., 2023, **3**, 970–990 | **987**

75 P. Verdugo, Marine microgels, *Annu. Rev. Mar. Science*, 2012, **4**, 375–400, DOI: **10.1146/annurev-marine-120709-142759**.

76 S. J. Biller, F. Schubotz, S. E. Roggensack, A. W. Thompson, R. E. Summons and S. W. Chisholm, Bacterial vesicles in marine ecosystems, *Science*, 2014, **343**, 183–186, DOI: **10.1126/science.1243457**.

77 M. V. Santander, Insights into Ocean-To-Atmosphere Transfer of Humic-like Substances and Bacteria, PhD thesis, University of California San Diego, U.S.A., p. 192, 2022.

78 C. Lee, C. M. Sultana, D. B. Collins, M. V. Santander, J. L. Axson, F. Malfatti, G. C. Cornwell, J. R. Grandquist, G. B. Deane, M. D. Stokes, F. Azam, V. H. Grassian and K. A. Prather, Advancing model systems for fundamental laboratory studies of sea spray aerosol using the microbial loop, *J. Phys. Chem. A*, 2015, **119**, 8860–8870, DOI: **10.1021/acs.jpca.5b03488**.

79 J. A. Fuhrman and R. T. Noble, Viruses and protists cause similar bacterial mortality in coastal seawater, *Limnol. Oceanogr.*, 1995, **40**, 1236–1242, DOI: **10.4319/lo.1995.40.7.1236**.

80 H. Ogawa, Y. Amagai, I. Koike, K. Kaiser and R. Benner, Production of refractory dissolved organic matter by bacteria, *Science*, 2001, **292**, 917–920, DOI: **10.1126/science.1057627**.

81 E. K. Wilbourn, D. C. O. Thornton, C. Ott, J. Graff, P. K. Quinn, T. S. Bates, R. Betha, L. M. Russell, M. J. Behrenfeld and S. D. Brooks, Ice nucleation by marine aerosols over the North Atlantic Ocean in late spring, *J. Geophys. Res.: Atmos.*, 2020, **125**, e2019JD030913, DOI: **10.1029/2019JD030913**.

82 N. J. Gotelli and R. K. Colwell, Quantifying biodiversity: procedures and pitfalls in the measurement and comparison of species richness, *Ecol. Lett.*, 2001, **4**, 379–391, DOI: **10.1046/j.1461-0248.2001.00230.x**.

83 A. Buchan, G. R. LeCleir, C. A. Gulvik and J. M. González, Master recyclers: features and functions of bacteria associated with phytoplankton blooms, *Nat. Rev. Microbiol.*, 2014, **12**, 686–698, DOI: **10.1038/nrmicro3326**.

84 H. P. Grossart, F. Levold, M. Allgaier, M. Simon and T. Brinkhoff, Marine diatom species harbour distinct bacterial communities, *Environ. Microbiol.*, 2005, **7**, 860–873, DOI: **10.1111/j.1462-2920.2005.00759.x**.

85 J. Pinhassi, M. M. Sala, H. Havskum, F. Peters, O. Guadayol, A. Malits and C. Marrasé, Changes in bacterioplankton composition under different phytoplankton regimens, *Appl. Environ. Microbiol.*, 2004, **70**, 6753–6766, DOI: **10.1128/AEM.70.11.6753-6766.2004**.

86 H. Teeling, B. M. Fuchs, D. Becher, C. Klockow, A. Gardebrecht, C. M. Bennke, M. Kassabgy, S. Huang, A. J. Mann, J. Waldmann, M. Weber, A. Klindworth, A. Otto, J. Lange, J. Bernhardt, C. Reinsch, M. Hecker, J. Peplies, F. D. Bockelmann, U. Callies, G. Gerdts, A. Wichels, K. H. Wiltshire, F. O. Glöckner, T. Schweder and R. Amann, Substrate-controlled succession of marine bacterioplankton populations induced by a phytoplankton

bloom, *Science*, 2012, **336**, 608–611, DOI: **10.1126/science.1218344**.

87 F. Thomas, J.-H. Hehemann, E. Rebuffet, M. Czjzek and G. Michel, Environmental and gut Bacteroidetes: the food connection, *Front. Microbiol.*, 2011, **2**, 16, DOI: **10.3389/fmicb.2011.00093**.

88 J.-H. Wang, J. Lu, Y.-X. Zhang, J. Wu, C. Zhang, X. Yu, Z. Zhang, H. Liu and W.-H. Wang, High-throughput sequencing analysis of the microbial community in coastal intensive mariculture systems, *Aquacult. Eng.*, 2018, **83**, 93–102, DOI: **10.1016/j.aquaeng.2018.10.001**.

89 M. Cunliffe, A. S. Whiteley, H. Schäfer, L. Newbold, A. Oliver and J. C. Murrell, Comparison of bacterioneuston and bacterioplankton dynamics during a phytoplankton bloom in a fjord mesocosm, *Appl. Environ. Microbiol.*, 2009, **75**, 7173–7181, DOI: **10.1128/AEM.01374-09**.

90 A. Krolicka, C. Boccadoro, M. M. Nilsen and T. Baussant, Capturing early changes in the marine bacterial community as a result of crude oil pollution in a mesocosm experiment, *Microbes Environ.*, 2017, **32**, 358–366, DOI: **10.1264/jsme2.ME17082**.

91 M. Cunliffe, A. Engel, S. Frka, B. Gašparović, C. Guitart, J. C. Murrell, M. Salter, C. Stolle, R. Upstill-Goddard and O. Wurl, Sea surface microlayers: a unified physicochemical and biological perspective of the air–ocean interface, *Prog. Oceanogr.*, 2013, **109**, 104–116, DOI: **10.1016/j.pocean.2012.08.004**.

92 J. Y. Aller, M. R. Kuznetsova, C. J. Jahns and P. F. Kemp, The sea surface microlayer as a source of viral and bacterial enrichment in marine aerosols, *J. Aerosol Sci.*, 2005, **36**, 801–812, DOI: **10.1016/j.jaerosci.2004.10.012**.

93 E. Rastelli, C. Corinaldesi, A. Dell'Anno, M. Lo Martire, S. Greco, M. C. Facchini, M. Rinaldi, C. O'Dowd, D. Ceburnis and R. Danovaro, Transfer of labile organic matter and microbes from the ocean surface to the marine aerosol: an experimental approach, *Sci. Rep.*, 2017, **7**, 1–10, DOI: **10.1038/s41598-017-10563-z**.

94 K. Engelhardt, A. Rumpel, J. Walter, J. Dombrowski, U. Kulozik, B. Braunschweig and W. Peukert, Protein adsorption at the electrified air–water interface: implications on foam stability, *Langmuir*, 2012, **28**, 7780–7787, DOI: **10.1021/la301368v**.

95 J. R. Lu, T. J. Su and J. Penfold, Adsorption of serum albumins at the air/water interface, *Langmuir*, 1999, **15**, 6975–6983, DOI: **10.1021/la990131h**.

96 J. S. Lee, B. M. Weon, S. J. Park, J. H. Je, K. Fezzaa and W.-K. Lee, Size limits the formation of liquid jets during bubble bursting, *Nat. Commun.*, 2011, **2**, 367, DOI: **10.1038/ncomms1369**.

97 E. R. Lewis and S. E. Schwartz, *Sea Salt Aerosol Production: Mechanisms, Methods, Measurements and Models – a Critical Review*, American Geophysical Union, Washington, DC, 2004, DOI: **10.1029/GM152**.

98 F. Veron, Ocean Spray, *Annu. Rev. Fluid. Mech.*, 2015, **47**, 507–538, DOI: **10.1146/annurev-fluid-010814-014651**.

99 C. F. Brasz, C. T. Bartlett, P. L. Walls, E. G. Flynn, Y. E. Yu and J. C. Bird, Minimum size for the top jet drop from

a bursting bubble, *Phys. Rev. Fluids*, 2018, **3**, 074001, DOI: **10.1103/PhysRevFluids.3.074001**.

100 R. L. Modini, L. M. Russell, G. B. Deane and M. D. Stokes, Effect of soluble surfactant on bubble persistence and bubble-produced aerosol particles, *J. Geophys. Res.: Atmos.*, 2013, **10**, 1388–1400, DOI: **10.1002/jgrd.50186**.

101 D. Dey, J. M. Boulton-Stone, A. N. Emery and J. R. Blake, Experimental comparisons with a numerical model of surfactant effects on the burst of a single bubble, *Chem. Eng. Sci.*, 1997, **52**, 2769–2783, DOI: **10.1016/S0009-2509(97)00083-3**.

102 P. K. Quinn, D. B. Collins, V. H. Grassian, K. A. Prather and T. S. Bates, Chemistry and related properties of freshly emitted sea spray aerosol, *Chem. Rev.*, 2015, **115**, 4383–4399, DOI: **10.1021/cr500713g**.

103 R. L. Stefan and A. J. Szeri, Surfactant scavenging and surface deposition by rising bubbles, *J. Colloid Interface Sci.*, 1999, **212**, 1–13, DOI: **10.1006/jcis.1998.6037**.

104 M. van Pinxteren, T.-B. Robinson, S. Zeppenfeld, X. Gong, E. Bahlmann, K. Wadinga Fomba, N. Triesch, F. Stratmann, O. Wurl, A. Engel, H. Wex and H. Herrmann, High number concentrations of transparent exopolymer particles in ambient aerosol particles and cloud water – a case study at the tropical Atlantic Ocean, *Atmos. Chem. Phys.*, 2022, **22**, 5725–5742, DOI: **10.5194/acp-22-5725-2022**.

105 S. Christiansen, M. E. Salter, E. Gorokhova, Q. T. Nguyen and M. Bilde, Sea spray aerosol formation: laboratory results on the role of air entrainment, water temperature, and phytoplankton biomass, *Environ. Sci. Technol.*, 2019, **53**, 3107–13116, DOI: **10.1021/acs.est.9b04078**.

106 M. Kuznetsova, C. Lee, J. Aller and N. M. Frew, Enrichment of amino acids in the sea-surface microlayers at coastal and open ocean sites in the North Atlantic Ocean, *Limnol. Oceanogr.*, 2004, **49**, 1605–1619, DOI: **10.4319/lo.2004.49.5.1605**.

107 P. Roy, L. E. Mael, T. C. J. Hill, L. Mehndiratta, G. Peiker, M. L. House, P. J. DeMott, V. H. Grassian and C. S. Dutcher, Ice nucleating activity and residual particle morphology of bulk seawater and sea surface microlayer, *ACS Earth Space Chem.*, 2021, **5**, 1916–1928, DOI: **10.1021/acsearthspacechem.1c00175**.

108 X. Gong, H. Wex, M. V. Pinxteren, N. Triesch, K. W. Fomba, J. Lubitz, C. Stolle, T. B. Robinson, T. Müller, H. Herrmann and F. Stratmann, Characterization of aerosol particles at Cabo Verde close to sea level and at the cloud level-part 2: ice-nucleating particles in air, cloud and seawater, *Atmos. Chem. Phys.*, 2020, **20**, 1451–1468, DOI: **10.5194/acp-20-1451-2020**.

109 M. J. Wolf, M. Goodell, E. Dong, L. A. Dove, C. Zhang, L. J. Franco, C. Shen, E. G. Rutkowski, D. N. Narducci, S. Mullen, A. R. Babbin and D. J. Cziczo, A link between the ice nucleation activity and the biogeochemistry of seawater, *Atmos. Chem. Phys.*, 2020, **20**, 15341–15356, DOI: **10.5194/acp-20-15341-2020**.

110 P. K. Quinn, T. S. Bates, K. S. Schulz, D. J. Coffman, A. A. Frossard, L. M. Russell, W. C. Keene and D. J. Kieber, Contribution of sea surface carbon pool to organic matter enrichment in sea spray aerosol, *Nat. Geosci.*, 2014, **7**, 228–232, DOI: **10.1038/ngeo2092**.

111 L. M. Russell, L. N. Hawkins, A. A. Frossard, P. K. Quinn and T. S. Bates, Carbohydrate-like composition of submicron atmospheric particles and their production from ocean bubble bursting, *Proc. Natl. Acad. Sci. U.S.A.*, 2010, **107**, 6652–6657, DOI: **10.1073/pnas.0908905107**.

112 M. van Pinxteren, S. Barthel, K. W. Fomba, K. Müller, W. Von Tümpling and H. Herrmann, The influence of environmental drivers on the enrichment of organic carbon in the sea surface microlayer and in submicron aerosol particles – measurements from the Atlantic Ocean, *Elem. Sci. Anth.*, 2017, **5**, 35, DOI: **10.1525/elementa**.

113 E. S. Hasenecz, T. Jayarathne, M. A. Pendergraft, M. V. Santander, K. J. Mayer, J. Sauer, C. Lee, W. S. Gibson, S. M. Kruse, F. Malfatti, K. A. Prather and E. A. Stone, Marine bacteria affect saccharide enrichment in sea spray aerosol during a phytoplankton bloom, *ACS Earth Space Chem.*, 2020, **4**, 638–1649, DOI: **10.1021/acsearthspacechem.0c00167**.

114 S. Zeppenfeld, M. van Pinxteren, D. van Pinxteren, H. Wex, E. Berdalet, D. Vaqué, M. Dall'Osto and H. Herrmann, Aerosol marine primary carbohydrates and atmospheric transformation in the Western Antarctic Peninsula, *ACS Earth Space Chem.*, 2021, **5**, 1032–1047, DOI: **10.1021/acsearthspacechem.0c00351**.

115 M. C. Facchini, M. Rinaldi, S. Decesari, C. Carbone, E. Finessi, M. Mircea, S. Fuzzi, D. Ceburnis, R. Flanagan, E. D. Nilsson, G. de Leeuw, M. Martino, J. Woeltjen and C. D. O'Dowd, Primary submicron marine aerosol dominated by insoluble organic colloids and aggregates, *Geophys. Res. Lett.*, 2008, **35**, L17814, DOI: **10.1029/2008GL034210**.

116 M. V. Santander, B. A. Mitts, M. A. Pendergraft, J. Dinasquet, C. Lee, A. N. Moore, L. B. Cancelada, K. L. A. Kimble, F. Malfatti and K. A. Prather, Tandem fluorescence measurements of organic matter and bacteria released in sea spray aerosols, *Environ. Sci. Technol.*, 2021, **55**, 5171–5179, DOI: **10.1021/acs.est.0c05493**.

117 P. J. DeMott, R. H. Mason, C. S. McCluskey, T. C. J. Hill, R. J. Perkins, Y. Desyaterik, A. K. Bertram, J. V. Trueblood, V. H. Grassian, Y. Qiu, V. Molinero, Y. Tobo, C. M. Sultana, C. Lee and K. A. Prather, Ice nucleation by particles containing long-chain fatty acids of relevance to freezing by sea spray aerosols, *Environ. Sci. Process Impacts*, 2018, **20**, 1559–1569, DOI: **10.1039/C8EM00386F**.

118 R. J. Perkins, M. G. Vazquez de Vasquez, E. E. Beasley, T. C. J. Hill, E. A. Stone, H. C. Allen and P. J. DeMott, Relating structure and ice nucleation of mixed surfactant systems relevant to sea spray aerosol, *J. Phys. Chem. A*, 2020, **124**, 8806–8821, DOI: **10.1021/acs.jpca.0c05849**.

119 M. Ardyna, H. Claustre, J.-B. Sallée, F. D'Ovidio, B. Gentili, G. van Dijken, F. D'Ortenzio and K. R. Arrigo, Delineating environmental control of phytoplankton biomass and

© 2023 The Author(s). Published by the Royal Society of Chemistry

Environ. Sci.: Atmos., 2023, **3**, 970–990 | **989**

phenology in the Southern Ocean, *Geophys. Res. Lett.*, 2017, **44**, 5016–5024, DOI: **10.1002/2016GL072428**.

120 J. Robinson, E. E. Popova, M. A. Srokosz and A. Yool, A tale of three islands: downstream natural iron fertilization in the Southern Ocean, *J. Geophys. Res.: Oceans*, 2016, **121**, 3350–3371, DOI: **10.1002/2015JC011319**.

121 C. M. S. Schine, A.-C. Alderkamp, G. van Dijken, L. J. A. Gerringa, S. Sergi, P. Laan, H. van Haren, W. H. van de Poll and K. R. Arrigo, Massive Southern Ocean phytoplankton bloom fed by iron of possible hydrothermal origin, *Nat. Commun.*, 2021, **12**, 1211, DOI: **10.1038/s41467-021-21339-5**.